Oxidation of bromide ions by hydroxyl radicals: Spectral characterization of the intermediate BrOH•-

Isabelle Lampre, Jean-Louis Marignier, Malaknaz Mirdamadi-Esfahani, Pascal Pernot, Pierre Archirel, Mehran Mostafavi

Oxidation of Bromide Ions by Hydroxyl Radicals: Spectral Characterization of the Intermediate $BrOH^{\bullet-}$

Isabelle Lampre[*], *Jean-Louis Marignier, Malaknaz Mirdamadi-Esfahani, Pascal Pernot, Pierre Archirel and Mehran Mostafavi*

Laboratoire de Chimie Physique, UMR 8000 CNRS / Université Paris-Sud,
Faculté des Sciences d'Orsay, Bât. 349, 91405 Orsay Cedex, France

ABSTRACT: The reaction of $^{\bullet}OH$ with Br^- has been re-investigated by picosecond pulse radiolysis combined with streak camera absorption detection and the obtained spectro-kinetics data have been globally analyzed using Bayesian data analysis. For the first time, the absorption spectrum of the intermediate species $BrOH^{\bullet-}$ has been determined. This species absorbs in the same spectral domain as $Br_2^{\bullet-}$: the band maximum is roughly at the same wavelength (λ_{max} = 352 nm instead of 354 nm) but the extinction coefficient is smaller (ε_{max} = 7800 ± 400 $dm^3\ mol^{-1}\ cm^{-1}$ compared with 9600 ± 300 $dm^3\ mol^{-1}\ cm^{-1}$) and the band is broader (88 nm versus 76 nm). Quantum chemical calculations have also been performed and corroborate the experimental results. In contrast to $Br_2^{\bullet-}$, the existence of several water-$BrOH^{\bullet-}$ configurations leading to different transition energies may account for the broadening of the absorption spectrum in addition to the higher number of degrees of freedom.

KEYWORDS: Pulse radiolysis, absorption spectrum, global analysis, quantum chemical calculations

1. INTRODUCTION

The oxidation of bromide ions, Br^-, and the subsequent formation of $Br_2^{\bullet-}$ and Br_3^- in aqueous solutions has been the subject of many radiolysis studies.[1-14] The dibromine radical anion ($Br_2^{\bullet-}$) is a strong oxidising radical characterized by a broad optical absorption band centred at 360 nm with an extinction coefficient, $\varepsilon_{max}(Br_2^{\bullet-})$, of 9900 ± 600 $dm^3\ mol^{-1}\ cm^{-1}$,[15] while the tribromine ion (Br_3^-) is a stable species which has an intense but narrow absorption spectrum located at 266 nm with , $\varepsilon_{max}(Br_3^-) = 40900 \pm 400\ dm^3\ mol^{-1}\ cm^{-1}$.[12, 16] It has been established that the oxidation of Br^- by the hydroxyl radical ($^{\bullet}OH$) is not a simple electron transfer reaction but involves the intermediate adduct $BrOH^{\bullet-}$. The latter may react with the hydronium cation (H_3O^+), dissociate to produce the bromine atom ($Br^{\bullet}$) as well as react with another Br^- and produce $Br_2^{\bullet-}$. The oxidation mechanism is in fact quite complex with reversible reactions:

$^{\bullet}OH + Br^- \rightleftharpoons BrOH^{\bullet-}$ $k_1 = (1.06 \pm 0.08) \times 10^{10}\ dm^3\ mol^{-1}\ s^{-1}$ [5] (R1)

$k_{-1} = (3.3 \pm 0.4) \times 10^7\ s^{-1}$ [5]

$BrOH^{\bullet-} \rightleftharpoons Br^{\bullet} + OH^-$ $k_2 = (4.2 \pm 0.6) \times 10^6\ s^{-1}$ [5] (R2)

$k_{-2} = 1.3 \times 10^{10}\ dm^3\ mol^{-1}\ s^{-1}$ [17, 18]

$BrOH^{\bullet-} + Br^- \rightleftharpoons Br_2^{\bullet-} + OH^-$ $k_3 = (1.9 \pm 0.3) \times 10^8\ dm^3\ mol^{-1}\ s^{-1}$ [5] (R3)

$k_{-3} = (2.7 \pm 0.5) \times 10^6\ dm^3\ mol^{-1}\ s^{-1}$ [8]

$BrOH^{\bullet-} + H_3O^+ \rightleftharpoons Br^{\bullet} (+ 2H_2O)$ $k_4 = (4.4 \pm 0.8) \times 10^{10}\ dm^3\ mol^{-1}\ s^{-11}$ [5] (R4)

$k_{-4} = 1.36\ s^{-1}$ [17]

$Br^{\bullet} + Br^- \rightleftharpoons Br_2^{\bullet-}$ $k_5 = (1.2 \pm 0.1) \times 10^{10}\ dm^3\ mol^{-1}\ s^{-1}$ [19] (R5)

$k_{-5} = 1.9 \times 10^4\ s^{-1}$ [19]

$Br_2^{\bullet-} + Br_2^{\bullet-} \longrightarrow Br_3^- + Br^-$ $k_6 = (1.9 \pm 0.1) \times 10^9\ dm^3\ mol^{-1}\ s^{-1}$ [9] (R6)

$Br_2 + Br^- \rightleftharpoons Br_3^-$ $K_7 = 16.1 \pm 0.3\ dm^3\ mol^{-1}$ [16] (R7)

The intermediate $BrOH^{\bullet-}$ was first suggested by Matheson, et al. [3] and then supported by works of Behar[6] and Zehavi and Rabani.[4, 5] While it was identified in irradiated frozen

aqueous solutions of alkali metal halides by electron spin resonance spectroscopy,[20] its optical characterization was not obvious and it was reported that $BrOH^{\bullet-}$ either does not absorb[6] or has an absorption similar to $Br_2^{\bullet-}$.[5] In the sixties, there were also some disagreements on the values of the rate constant of the reaction between $^{\bullet}OH$ and Br^-, mainly due to pH sensitivity of the system. Sutton et al. reported that, in contrast to the corresponding reaction with chloride ion, the reaction between $^{\bullet}OH$ and Br^- was exothermic and occurs rapidly even in neutral solution ($k_1 \geq 10^9$ $dm^3mol^{-1}s^{-1}$).[2] The pulse radiolysis of deaerated aqueous bromide solutions by Matheson at al. yielded the value $k_1 = (1.2 \pm 0.15) \times 10^9$ $dm^3mol^{-1}s^{-1}$.[3] Then, Zehavi and Rabani elucidated the mechanism of bromide oxidation by $^{\bullet}OH$ radicals and determined a tenfold higher value for k_1.[5] This value given above corresponds to the value now used as a reference.[21] Zehavi and Rababi attempted to measure the absorption spectrum of $BrOH^{\bullet-}$. They found that the absorption of the intermediate $BrOH^{\bullet-}$ is quite similar to that of $Br_2^{\bullet-}$; the spectrum of $BrOH^{\bullet-}$ exhibits a band around 360 nm broader than that of $Br_2^{\bullet-}$ and with a lower extinction coefficient.[5] Taking into account the absorbance of $BrOH^{\bullet-}$, Mamou et al. removed some discrepancies in the kinetics data.[8] Even if it is now admitted that $BrOH^{\bullet-}$ is an absorbing species,[10] to our knowledge its absorption spectrum has not yet been characterized. In this paper, we present a pulse radiolysis study of sodium bromide solution. Thanks to a new detection set-up based on a CCD camera with a high resolution and a global Bayesian data analysis, we were able to distinguish between $BrOH^{\bullet-}$ and $Br_2^{\bullet-}$ and determine the optical spectrum of the intermediate $BrOH^{\bullet-}$. Indeed, Bayesian data analysis has been used with success in the past years for the analysis of spectrokinetic data.[22-30] It has proved to be an essential tool to tackle parametric identification problems, which are omnipresent in the kinetic modeling of time-resolved spectra. Quantum calculations have also been performed for both species to provide some insights on the electronic transitions responsible of the absorption.

2. EXPERIMENTAL AND COMPUTATIONAL SECTION

Materials. The aqueous solutions were prepared using ultra-pure water from a Millipore system. The chemicals, sodium bromide NaBr (purity >99%) and acetone, were obtained from Sigma-Aldrich and used as received without further purification. The solutions were saturated with dinitrogen or argon (N_2, Ar, purity >99.995% from Air Liquide) by bubbling before and during experiments. The solutions with a natural pH around 5.5 were stable at

room temperature under room light. All solutions were irradiated at room temperature (~20°C).

Pulse radiolysis measurements. The experiments were carried out on the picosecond laser-triggered electron accelerator ELYSE at University Paris-Sud (Orsay) coupled with an absorption spectroscopic detection system.[31, 32] Electron pulses with 7.9 MeV energy, ~6 nC charge and 15 ps duration were delivered at a repetition rate of 2 Hz. The dose deposited in water was around 50 Gy in the irradiated volume (*i.e.* $[e_{aq}^-] \approx 2 \times 10^{-5}$ M). The studied sample was contained in a 10 × 10 mm irradiation quartz cell. A close circulation system from a 100 mL N_2-purged stock solution was used to renew the sample between each pulse (peristaltic pump, flow rate 80 mL/min). Absorption measurements were performed using the white light beam of a homemade Xenon flash lamp.[33] The light was focused through the sample collinearly with the electron beam and then directed onto the detection set-up which was composed of a spectrograph (Chromex 250IS) and a high dynamic range streak camera (Hamamatsu C7700-01). For this study, a 150 grooves/mm and 300 nm blaze grating and 200 µm slits were used and 20 ns, 50 ns or 500 ns sweep time/full screen were performed. For each flash, an image (1024 × 1344 pixels) resolved in time and wavelength (340 nm full screen) was acquired but to get a good signal to noise ratio series of 700 images were averaged in a unique image. Then, the time-resolved absorbance of the sample was calculated using average images obtained with and without the electron pulses. The full spectra from 300 to 590 nm were obtained by two series of absorption measurements using two different optical filters (UG 5 and GG325) to optimize the light intensity on a specific spectral domain (290 to 420 nm and 360 to 590 nm, respectively). The spectral overlap between 360 and 420 nm allows us to check the good stability and reproducibility of the irradiation measurements.

Bayesian data analysis. A general introduction on Bayesian data analysis can be found in Gregory's book,[34] and a more focused treatment on spectrokinetic data in the paper written by Ruckebusch and co-workers.[35] A minimal overview is provided here.

Bayesian data analysis is based on the *posterior* probability density function (pdf) $p(\theta|\mathbf{D},\mathrm{H})$, which is a N_θ-dimensional distribution over the values of a set of N_θ uncertain parameters θ, conditional to the values of the experimental data **D** and to an ensemble of hypotheses H. The *posterior* pdf can be built from available information through the Bayes theorem:

$$p(\theta|\mathbf{D},\mathrm{H}) \propto p(\mathbf{D}|\theta,\mathrm{H}) \times p(\theta|\mathrm{H}) \quad (1)$$

The function $p(\mathbf{D}|\theta,\mathrm{H})$ is called the *likelihood*; it describes the statistical model of measurement uncertainties, while the *prior* pdf $p(\theta|\mathrm{H})$ represents the state of knowledge on the parameters before analyzing the data. For the present study, the norm factor of the *posterior* pdf is not useful and has been left unspecified.

Technically, a search for the optimal parameter set, the so-called Maximum A Posteriori (MAP) parameters, is performed in order to assess the goodness-of-fit of the model and to provide a favorable starting point for the random walk (Markov Chain Monte Carlo, MCMC) through which a representative sample of the *posterior* pdf is generated by a Metropolis-Hastings algorithm.[36] Estimates of the parameters and their uncertainties are obtained from this sample.

In the present study, the experimental data images were downsized to a 70 × 70 spectrokinetics data matrix **D** with a final resolution of 3.4 ns and 2.7 nm. We used a hybrid spectrokinetic model M, where the kinetic traces are described by a parametric kinetic model and the spectra are treated non parametrically, as described by Ruckebusch et al.[35] The recovery of the spectra is affected by various sources of uncertainty: (i) data uncertainty (measurement noise, time and wavelength calibration), and (ii) uncertainty associated to the parameters of the spectrokinetic model and the model itself.

The first source of uncertainty is accounted for by a proper treatment of data noise by using a variance/covariance matrix in the *likelihood* function. In the present study, we assumed that the time and wavelength are known without random uncertainty. They might be affected by a systematic error without impact on the results of the present study. The data noise is heteroscedastic (not uniform) in wavelength for two reasons: composite image and camera sensitivity. Before downsizing the noise structure was analyzed in the time-asymptotic part of the image, where there is no/few signal evolution. For each wavelength channel, the standard deviation (corrected from a possible linear variation) was estimated over 200 time points of the raw data matrix (Supporting Information, blue dots in Figure S1). A wavelength-wise local linear regression (loess interpolation) of the noise amplitude was used as a proxy for the average noise amplitude used to calculate weighted residuals. In order to get a standard Gaussian distribution of the weighted residuals, we had to correct the noise amplitude by a multiplicative factor (1.4). This new noise level corresponds approximately to the wavelength-dependent upper bound of a symmetric 90 % confidence interval for the noise amplitude (Supporting Information, red curve in Figure S1). The *likelihood* function is expressed, up to its norm factor, as

$$p\left(\mathbf{D}\middle|\theta,\mathrm{M}\right)\propto\exp\left\{-\frac{1}{2}\sum_{l}\frac{1}{\sigma_l^2}\sum_{k}\left[D_{kl}-M_{kl}(\theta)\right]^2\right\} \quad (2)$$

where the indices *l* and *k* cover the wavelength and time grid, respectively, and σ_l represents the wavelength-dependent standard deviation of measurement noise.

For parametric uncertainty, we distinguish amongst *internal* parameters, θ_{int}, which are directly related to the conditions of the current data (initial concentrations of reagents, initial time calibration...), and *external* parameters, θ_{ext}, for which, in the case where the model is valid, we do not expect to gather information from the data. Initially, the rate constants are treated as *external* uncertain parameters, because it is not *a priori* obvious that there is enough information in the present data to get a reasonable inference on their values. *A contrario*, we include the absorption coefficient $\varepsilon_{max}(Br_2^{\bullet-})$ into the *internal* or Optimized Parameters Set (OPS), because its value in the experiment could be affected by the calibration of the dose, for instance. In the course of the analysis, the OPS might be augmented by recruiting parameters of the *external* set, until residuals analysis enables to conclude to a reasonable fit of the data.

As the parameters in the OPS are uncorrelated in the present study, the *prior* pdf is simply the product of the *prior* pdfs of the individual parameters:

$$p\left(\theta\middle|\mathrm{M}\right)=\prod_i p\left(\theta_i\middle|\mathrm{M}\right) \quad (3)$$

Monte Carlo Uncertainty Propagation (MCUP). Bayesian inference in the OPS is conditional to the values of the parameters in the *external* set. As the latter are uncertain, we have to check their influence on the inferred values. Expliciting the partition of the parameters, the *posterior* pdf for the parameters of the OPS can be noted $p(\theta_{int}|\theta_{ext},\mathbf{D},\mathrm{M})$, and the effect of the uncertainty in the *external* parameters obtained by Uncertainty Propagation (Markov Equation, see reference 37)

$$p\left(\theta_{int}\middle|\mathbf{D},\mathrm{M}\right)=\int d\theta_{ext}\,p\left(\theta_{int}\middle|\theta_{ext},\mathbf{D},\mathrm{M}\right)p\left(\theta_{ext}\middle|\mathrm{M}\right) \quad (4)$$

where the design of $p(\theta_{ext}|\mathrm{M})$ is similar to the *prior* pdf defined above.

Implementation of Equation 4 is commonly done by a Monte Carlo approach (noted MCUP thereafter), where a representative sample of the left hand side pdf is obtained by evaluating the *posterior* pdf for a representative sample of $p(\theta_{ext}|\mathrm{M})$. As the *posterior* pdf is itself obtained by Markov Chain Monte Carlo sampling, this results in a double Monte Carlo method, which is very computer intensive. We used here an approximation evaluating the

impact of p(θ_{ext}|M) on the Maximum A Posteriori for the *internal* parameters θ_{int}^{MAP}. This is often sufficient to appreciate the impact of the *external* parameters. An approximation of the total variance of the *internal* parameters, $u^2(\theta_{int})$, due to the data and *external* parameters can be obtained as:

$$u^2(\theta_{int}) = u^2\left(\theta_{int}\left|\theta_{ext},\mathbf{D}\right.\right) + u^2\left(\theta_{int}^{MAP}\left|\mathbf{D}\right.\right) \quad (5)$$

where θ_{ext} denotes the nominal value of the corresponding *external* parameters.

All calculations have been performed with the R language.[38] URL http://www.R-project.org/ #71

URL http://www.R-project.org/ #71

Quantum calculations for transition energies. To determine the electronic transitions of $BrOH^{\bullet-}$ and $Br_2^{\bullet-}$ in aqueous solution, the systems $Br_2^{\bullet-}(H_2O)_n$ and $BrOH^{\bullet-}(H_2O)_n$, with n small were studied using a conventional TDDFT method on a set of configurations and modeling the solvent with a PCM reaction field in the SMD formalism. The SDD core pseudo-potentials and basis sets were used supplemented with polarization Gaussians on all atoms: one d on O atoms (exponent: 0.8) and Br atoms (0.3) and one p on H atoms (1.1).[39] This polarized SDD basis set is noted pSDD. All calculations were carried out with the Gaussian 09 program[40] and Molpro *ab initio* program[41] packages.

3. RESULTS AND DISCUSSION

Pulse radiolysis. Radiolysis of neutral aqueous solutions mainly generates hydrated electrons (e_{aq}^-), hydroxyl radicals ($^{\bullet}OH$) and hydrogen atom ($H^{\bullet}$). $^{\bullet}OH$ and $H^{\bullet}$ absorb weakly far in the UV spectral domain [21] and will not be detected above 300 nm, our spectral domain of interest. In contrast, e_{aq}^- presents a strong and very broad absorption band centred at 720 nm which overlaps the spectral domain of $Br_2^{\bullet-}$ absorption. Indeed, the molar extinction coefficient of e_{aq}^- at 360 nm ($\varepsilon_{360\ nm}(e_{aq}^-)$ = 1790 $dm^3\ mol^{-1}\ cm^{-1}$) is roughly one fifth of that of $Br_2^{\bullet-}$. In order to get rid of the e_{aq}^- contribution to the absorption signals, acetone was used to scavenge the hydrated electron as the formed alcohol radical, $(CH_3)_2C^{\bullet}OH$, hardly absorbs in the explored spectral domain (ε < 500 $dm^3\ mol^{-1}\ cm^{-1}$ for λ > 300 nm): [42, 43]

$$e_{aq}^- + (CH_3)_2CO \longrightarrow (CH_3)_2C^{\bullet}O^- \qquad k_8 = 6.5 \times 10^9\ dm^3\ mol^{-1}\ s^{-1}\ [21] \qquad (R8)$$

$$(CH_3)_2C^{\bullet}OH \rightleftharpoons (CH_3)_2C^{\bullet}O^- + H^+ \qquad pK_a = 12\ [44] \qquad (R9)$$

$^{\bullet}OH$ can also react with acetone but the rate constant is two orders of magnitude lower than that of reaction R1 with Br^-:

$$^{\bullet}OH + (CH_3)_2CO \longrightarrow \text{products} \qquad k_{10} = 1.3 \times 10^8 \text{ dm}^3 \text{ mol}^{-1} \text{ s}^{-1} \ ^{45} \qquad \text{(R10)}$$

The generated products do not absorb in the studied spectral domain. Indeed, pulse-radiolysis of Ar-purged aqueous solutions containing acetone alone shows only a weak absorption due to $(CH_3)_2C^{\bullet}OH$ generated by R8-9 (Supporting Information, Figure S2).

It is to be noted that N_2O-saturated solution (2.5×10^{-2} M N_2O) could have been used to convert e_{aq}^- into $^{\bullet}OH$:

$$e_{aq}^- + N_2O \longrightarrow N_2 + O^{\bullet-} \qquad k_{10} = 9.1 \times 10^9 \text{ dm}^3 \text{ mol}^{-1} \text{ s}^{-1} \ ^{21} \qquad \text{(R11)}$$

$$O^{\bullet-} + H_2O \rightleftharpoons {}^{\bullet}OH + OH^- \qquad pK_a = 11.9 \ ^{21} \qquad \text{(R12)}$$

But, these reactions would have produced $^{\bullet}OH$ for roughly 4.5 ns, what would have complicated the kinetics analysis on the nanosecond time scale.

Figure 1 shows the time evolution of the optical absorption spectrum obtained by pulse radiolysis of N_2-purged aqueous solutions containing 0.01 M NaBr and 0.1 M acetone. The optical absorption spectrum registered 0.85 ns after the electron pulse (Figure 1, red) presents two bands: one band located around 360 nm and one band above 450 nm. While the band around 360 nm rises with time, the band in the red decreases rapidly and vanishes. After 10 ns, the spectra present only the absorption band around 360 nm which reaches a maximum at ~300 ns. The band above 450 nm is due to the hydrated electrons (e_{aq}^-) which disappears by reaction R8 with acetone. The band around 360 nm is associated with the oxidation of Br^- and the formation of $BrOH^{\bullet-}$ and $Br_2^{\bullet-}$.

The time dependence of absorbance at different wavelengths: 305, 360, 400 and 570 nm are shown on Figure 2. The absorption signal at 570 nm (Figure 2a, orange) due to the hydrated electron rises during the electron pulse and then decays exponentially. A pseudo-first order rate constant for the disappearance of e_{aq}^- is found to be 6.7×10^8 s^{-1}. Taking into account the concentration of acetone, that corresponds to a bimolecular rate constant of 6.7×10^9 $dm^3 \, mol^{-1} \, s^{-1}$; this value is in the range (from 5.6×10^9 $dm^3 \, mol^{-1} \, s^{-1}$ to 8×10^9 $dm^3 \, mol^{-1} \, s^{-1}$) of the reported values[46-51] and in good agreement with the average selected value (6.5×10^9 $dm^3 \, mol^{-1} \, s^{-1}$)[21] of k_8. Regarding the signals registered at 360, 305 and 400 nm *i.e.* near the absorption maximum and on the blue and red side of the absorption band, the kinetics profiles are clearly wavelength dependent. Whatever the wavelength, an absorbance

has built up during the electron pulse duration and the signals present a fast rise for about 15 ns (Figure 2a) showing the very fast formation of an absorbing species. Then, the signal at 305 nm decays slowly and the absorbance at 400 nm remains nearly constant while the signal at 360 nm continues to grow regularly till 300 ns to reach a plateau in our explored time window (Figure 2b). The fast rise in absorbance during the pulse duration is partly due to the production of e_{aq}^- but also attributed to reaction R1 and the appearance of $BrOH^{\bullet-}$. The fast increase in the signals at wavelength below 425 nm is also associated with the formation of $BrOH^{\bullet-}$ whereas the following slow evolutions (increase at 360 nm, decay at 305 nm) are related to the formation of $Br_2^{\bullet-}$ at the expense of $BrOH^{\bullet-}$.

Figures 3 and 4 depict the spectral changes and kinetics profiles obtained by pulse radiolysis of N_2-purged aqueous solutions containing 0.05 M NaBr and 0.1 M acetone. The observed changes are similar to those just described for 0.01 M NaBr solution, but on a shorter time scale. As expected by the increase in Br^- concentration, the formation kinetics of $BrOH^{\bullet-}$ and $Br_2^{\bullet-}$ are accelerated. In addition, under these conditions, after 200 ns the absorbance at 360 nm starts to decay slightly due to the slow disappearance of $Br_2^{\bullet-}$ and the formation of Br_3^- according to reaction R6.

Those results corroborate the kinetics and spectral measurements performed by Zehavi and Rabani[5] and confirm their overall statement that the intermediate $BrOH^{\bullet-}$ absorbs in the same spectral domain as $Br_2^{\bullet-}$ but with a broader spectrum. Indeed, the normalized absorption spectra recorded at 10 ns and 400 ns for the solution containing 0.01 M NaBr and 0.1 M acetone are clearly not identical (Figure 1b). While the spectrum at 400 ns is close to the absorption spectrum reported for $Br_2^{\bullet-}$, the spectrum at 10 ns seems slightly shifted to the blue and much broader. It is to be noted that a broader spectrum for $BrOH^{\bullet-}$ compared with $Br_2^{\bullet-}$ is not surprising because $BrOH^{\bullet-}$ is a triatomic ion with more degrees of freedom than the diatomic $Br_2^{\bullet-}$ anion and with the ability of H-bond formation with the solvent water molecules, what may induce many solvation micro-environment and energy differences.

Bayesian data analysis. The spectrokinetic data obtained for aqueous solutions containing 0.01 M NaBr and 0.1 M acetone have been analyzed using a Bayesian method for parametric identification. Singular Value Decomposition of the data matrix indicates that its rank is 2. Considering the strong overlap of the candidate spectra, rotational ambiguity prevents the recovering of unique spectra, even when positivity and/or unimodality constraints are

enforced.[35] In order to reduce the solution space, we used an explicit model of the kinetic traces taking into account reactions/equilibriums R1 to R6, R8 and R10.
In the present case, the model M of the absorbance data matrix is:

$$M_{lk} = S_{BrOH^{\bullet-}}(\lambda_l) \times C_{BrOH^{\bullet-}}(t_k + \delta t) + S_{Br_2^{\bullet-}}(\lambda_l) \times C_{Br_2^{\bullet-}}(t_k + \delta t) + n_{lk} \quad (4)$$

where $C_{BrOH^{\bullet-}}(t_k + \delta t)$ and $C_{Br_2^{\bullet-}}(t_k + \delta t)$ represent the time-dependent concentration of $BrOH^{\bullet-}$ and $Br_2^{\bullet-}$, respectively; δt is an small time-shift compensating for the uncertainty in the exact initial time due to the width of the Cherenkov dip, and n_{lk} is a random variable representing measurement noise. The spectra of both species, $S_{BrOH^{\bullet-}}(\lambda_l)$ and $S_{Br_2^{\bullet-}}(\lambda_l)$, which correspond to the extinction coefficients, $\varepsilon\lambda(BrOH^{\bullet-})$ and $\varepsilon\lambda(Br_2^{\bullet-})$, multiplied by the optical path length (equal to 1 cm in our case), are obtained wavelength-wise by linear regression. The maximum absorption coefficient of $S_{Br_2^{\bullet-}}$, $\varepsilon_{max}(Br_2^{\bullet-})$, is constrained around 9900 ± 300 $dm^3\ mol^{-1}\ cm^{-1}$, while $S_{BrOH^{\bullet-}}$ is left unconstrained except positivity. The homogeneous chemistry model used to model the kinetic traces is not designed to reproduce the short-time kinetics of the system and the matrix model M (Eq. 4) does not take into account the absorption of the solvated electron. Consequently, the analyzed data matrix is restricted to the time range above 20 ns (the exact value depends on the zero-time shift parameter δt) when the solvated electron has vanished.

The kinetic traces are calculated by numerical integration of the kinetic model (R1 – R6, R8, R10), with the initial concentrations: $[H_3O^+]_0 = [e_{aq}^-]_0 = 2 \times 10^{-5}$ M, $[(CH_3)_2CO]_0 = 0.1$ M, $[OH^{\bullet}]_0 = 2 \times 10^{-5}$ M and $[Br^-]_0 = 0.01$ M. The latter two initial concentrations are treated as uncertain with 20% and 5% relative uncertainty, respectively.

In order to get estimation of the spectra and of their uncertainty, we proceeded in 5 steps:

(1) identification of the Maximum A Posteriori (MAP) parameters with the initial Optimized Parameters set (OPS) and validation of the model (analysis of residuals);
(2) in the presence of improper residuals, addition of new parameters in the OPS on the basis of a sensitivity analysis;
(3) identification of the MAP parameters with the augmented OPS and validation of the model (analysis of residuals);
(4) generation of the possible set of spectra compatible with the full *posterior* pdf of the OPS;

(5) study of the influence of the *external* parameters on the recovered spectra called Monte Carlo Uncertainty Propagation (MCUP).

(1) A first attempt was performed with an OPS including four parameters (δt, $[OH^\bullet]_0$, $[Br^-]_0$ and $\varepsilon_{max}(Br_2^{\bullet-})$). The details on the *prior* pdfs of the parameters and the results, MAP1, are reported in Table 1: a rather good optimal point could be obtained (χ^2_R=1.06, *P*=0.01), with normally distributed residuals. However, the analysis of the residual map revealed a significant structure along the time axis. After considering and rejecting various error sources, we decided to resolve this residual structure by relaxing a minimal set of reaction rate constants.

(2) The minimal set of relevant rate constants was obtained by sensitivity analysis (SA) of the estimated $BrOH^{\bullet-}$ spectrum vs. all uncertain parameters, for which a sample of 500 draws was generated from their *prior* pdf. The $BrOH^{\bullet-}$ spectrum at 20 wavelengths between 300 and 500 nm was generated for each point of the sample. We used an ANOVA-SA type approach:[52] the sensitivity coefficients are the fractions of the total output variance apportioned to each input variable. They are obtained analytically from a quadratic least-squares fit of the response as a function of the inputs. We adapted a procedure proposed by Zhang and Goutsias[53] to the case of inputs with non-Gaussian densities.[54] Among the reaction rates, k_1, k_{-1}, k_2 and k_{10} stand out (Supporting Information, Figure S3). Although k_{-1} has a rather uniform sensitivity index across the wavelength scale, k_2 and k_{10} seem to contribute mostly near the wings of the spectrum. These reaction rate constants have been included in the OPS.

(3) The optimization process was repeated with the augmented OPS (8 parameters) and lead to a new optimal set MAP2 (Table 1). The improvement of the χ^2_R is significant (χ^2_R=1.02, *P*=0.13), and the structure in the residuals has vanished (Figure 5). The model can be considered as statistically valid, and we can now sample the *posterior* pdf of the parameters. The spectra and time-dependent concentrations of $Br_2^{\bullet-}$ and $BrOH^{\bullet-}$ obtained at this analytical step are given in Figure S4, Supporting Information.

(4) A *posterior* sample was generated for the 8 parameters in the OPS (see section 2), and 1000 points were retained to evaluate the mean and standard deviation of the parameters (Table 1). The corresponding set of 1000 numerical spectra for $Br_2^{\bullet-}$ and $BrOH^{\bullet-}$ (Figure 6) has been used to estimate spectral properties by quadratic fit of the log-spectra in the energy scale. The statistics for these results are reported in Table 2. Note that the quadratic model cannot accommodate a hump near the maximum of $Br_2^{\bullet-}$, which provides an underestimation

of $\varepsilon_{max}(Br_2^{\bullet-})$ by this procedure, when compared with the (preferred) value reported in Table 1.

(5) Finally, the influence of the external parameters (k_{-2}, k_3, k_{-3}, k_4, k_{-4}, k_5, k_{-5}, k_6 and k_8) was studied by repeating the MAP2 identification, step (3), for a random sample of values of these parameters, drawn from their *prior* pdf (MCUP sampling). The *prior* pdfs of the *external* rate constants are *Lognormal* distributions using the mean value and uncertainty factor reported in the literature or taken as 20%. As can be seen in Tables 1 and 2, the mean values of the MCMC and MCUP procedures are statistically compatible. Moreover, the uncertainty of the inferred parameters due to the *external* parameters is never larger than the uncertainty obtained by the MCMC procedure, which confirms that the important parameters are effectively in the MAP2-OPS. The uncertainties reported at the MCMC stage can be considered as representative, but in the few cases where both uncertainties are of similar amplitudes, one could use the combination of variances to derive an overall uncertainty. For instance, the global uncertainty on $\varepsilon_{max}(BrOH^{\bullet-})$ could be estimated as $(365^2 + 140^2)^{1/2} = 390$ dm^3 mol^{-1} cm^{-1}.

To summarize, the spectrum of $BrOH^{\bullet-}$ could be differentiated from that of $Br_2^{\bullet-}$ (Table 2 and Figure 6). Both spectra peak at similar wavelength (352 vs. 354 nm), but the molar absorption coefficient of $BrOH^{\bullet-}$ at its maximum is 7800 ± 400 dm^3 mol^{-1} cm^{-1}, significantly smaller than $\varepsilon_{max}(Br_2^{\bullet-})$. However, the spectrum of $BrOH^{\bullet-}$ is significantly wider (fwhm = 88 vs. 76 nm) and both species have nearly identical oscillator strengths (ratio $OS(BrOH^{\bullet-})/OS(Br_2^{\bullet-}) = 0.95 \pm 0.03$). Our results confirm the general trends of the work of Zehavi and Rabani.[5] In their attempt to measure the absorption spectrum of $BrOH^{\bullet-}$, they determined absorbance ratios at a few wavelengths and deduced that the $BrOH^{\bullet-}$ peak seemed broader than the $Br_2^{\bullet-}$ peak; they also estimated the extinction coefficient of $BrOH^{\bullet-}$ to be about 8000 dm^3 mol^{-1} cm^{-1} but with an extinction coefficient of 12000 dm^3 mol^{-1} cm^{-1} for $Br_2^{\bullet-}$. However, it is worth noticing that the position of the maximum of $Br_2^{\bullet-}$ absorption spectrum is found slightly blue-shifted compared to the reference value (354 instead of 360 nm) but that this position is in agreement with recent measurements.[14] Moreover, it is to be noted that the rate constants k_1 and k_2 have also been slightly adjusted from the literature values and found to be $k_1 = (8.4 \pm 0.5) \times 10^9$ dm^3 mol^{-1} s^{-1} and $k_2 = (8.2 \pm 0.6) \times 10^{10}$ dm^3 mol^{-1} s^{-1}.

Quantum calculations. The simulation of the two species $Br_2^{\bullet-}$ and $BrOH^{\bullet-}$ in solution is difficult because of the quantum resonance between two mesomeric forms, $BrBr^-$ and Br^-Br in the first case, $BrOH^-$ and Br^-OH in the second case. This makes the elaboration of a classical force field difficult. In a first attempt, we performed CPMD simulations of the solutes with 64 water molecules and found that the interatomic distances of the solutes were unrealistically large and the transition energies much too small.[55] Then, we performed QMMM simulations with a PM3 solute and 250 classical water molecules and found that conversely the interatomic distances of the solutes were unrealistically small.[55] Thus, we used a conventional DFT method with optimization of a set of configurations of the systems $Br_2^{\bullet-}(H_2O)_n$ and $BrOH^{\bullet-}(H_2O)_n$, with n small and the remaining of the solvent modeled with a PCM reaction field in the SMD formalism.[40]

As a preliminary step, for $Br_2^{\bullet-}$, we compared two functionals of the literature: BHHLYP which had already been used on the $Br_2^{\bullet-}(H_2O)_n$ system in the vacuum[56] and B3LYP.[57] We used the pSDD basis set and tested the addition of diffuse Gaussians: s (exponents 0.07, 0.03, 0.01) and p (exponents 0.02, 0.01). Table 3 gives the excitation energy obtained for $Br_2^{\bullet-}$. It was found that adding diffuse functions had no effect on the calculated excitation energy of $Br_2^{\bullet-}$ and that the B3LYP results were closer to the experimental value (around 360 nm) than the BHHLYP value (Table 3). Consequently, we used B3LYP and the pSDD basis set for all the systems.

First, we calculated the transition energies of the solutes with zero explicit water molecules (Tables 4 and 5). This means that the solvent is completely modeled by the PCM method. It is found that the two solutes absorb at different wavelengths, with the $Br_2^{\bullet-}$ transition energy (3.33 eV, 372 nm) significantly larger than the $BrOH^{\bullet-}$ one (3.07 eV, 404 nm). These two values differ from the observed value for both solutes (around 3.49 eV, 355 nm). Moreover, the oscillator strength of $Br_2^{\bullet-}$ (0.45) is larger than the oscillator strength of $BrOH^{\bullet-}$ (0.34), but the ratio of these values amounts to 0.75, in qualitative agreement with the measured value (0.9). The present TDDFT calculations yield absorption lines and no band widths. Nevertheless we note that the $Br_2^{\bullet-}$ solute has six degrees of freedom in the solvent cage while $BrOH^{\bullet-}$ has nine. For this reason we may expect that the absorption band of $BrOH^{\bullet-}$ is larger than that of $Br_2^{\bullet-}$. This is in agreement with the measurements.

Then, we considered the solutes with a coating of one explicit water molecule. In this case the two solutes display different behaviors: $Br_2^{\bullet-}$ takes up the water molecule in one way only (Figure 7), $BrOH^{\bullet-}$ in three different ways, with the hydrogen bond of the types $W \rightarrow OH$,

W → Br and W ← OH (Figure 8), where W stands for the water molecule. In Table 5 are reported the binding mode of the three $BrOH^{\bullet-}(H_2O)$ configurations and the number of equivalent configurations, n_{conf}, as well as the relative energy of the three $BrOH^{\bullet-}(H_2O)$ configurations. These energies ($\Delta G_i = G_i - G_1$) have been calculated according to:

$$G_i = G_i^{DFT} + \Delta E_i^{CCSD} - RTLn\ n_{conf} \quad (5)$$

$$\Delta E_i^{CCSD} = E_i^{CCSD} - E_i^{DFT} \quad (6)$$

where G^{DFT} is the B3LYP/PCM electronic and nuclear free energy of the solute; $RTLn\ n_{conf}$ is the conformation entropy of the configuration. ΔE^{CCSD} is a correction using E_i^{DFT}, the B3LYP energy of the solute in the vacuum and E_i^{CCSD}, the CCSD(T) energy in the aug-cc-pvqz basis of the same system.[41]

While the three $BrOH^{\bullet-}(H_2O)$ configurations lie within 0.08 eV (Table 5), it is striking that these configurations display different absorption wavelengths, between 368 nm (W → OH, ground configuration) and 398 nm (W ← OH). This feature is certainly an additional cause of the broader band of $BrOH^{\bullet-}$ compared with $Br_2^{\bullet-}$.

We also considered coated solutes with 2, 3 and 4 explicit water molecules. In each case we took into account only one configuration, with the lowest energy (Figures 7 and 8). The results converge as soon as n = 2 – 3 (Tables 4 and 5). For n = 2 the absorption wavelengths of $Br_2^{\bullet-}(H_2O)_2$ (360 nm) is larger than that of $BrOH^{\bullet-}(H_2O)_2$ (354 nm). Note that the corresponding transition energies differ by 0.06 eV only. According to the present measurements the two solutes absorb at similar wavelengths. Nevertheless, these two solutes are different ions and there is no reason for the absorption wavelengths to be equal. Our results suggest that the absorption wavelength of $Br_2^{\bullet-}$ is slightly larger than that of $BrOH^{\bullet-}$, but it is worth noticing that these results correspond to the lowest energy configuration only. Figure 9 shows the absorption spectra of the two solutes deduced from the last values (with n = 3) and a convolution using two different Gaussians with full widths at half maximum (fwhm) of 0.75 and 0.9 eV for $Br_2^{\bullet-}$ and $BrOH^{\bullet-}$, respectively. These fwhm values are empirically taken from the measurements.

4. CONCLUSION

In the present work, the absorption spectrum of $BrOH^{\bullet-}$ has been investigated both experimentally by pulse radiolysis and theoretically. The measurements and data analysis indicate that $BrOH^{\bullet-}$ absorbs at a similar wavelength as $Br_2^{\bullet-}$ but presents a broader absorption

band with a lower molar extinction coefficient (7800 ± 400 dm^3 mol^{-1} cm^{-1} compared with 9600 ± 300 dm^3 mol^{-1} cm^{-1}). Quantum chemistry calculations performed on both species corroborate the absorption of $BrOH^{\bullet-}$ in the same spectral region as $Br_2^{\bullet-}$. They also reveal the existence of different water-$BrOH^{\bullet-}$ configurations with different transition energies, what may account for the broadening of the spectrum.

ASSOCIATED CONTENT

Supporting Information

Data noise analysis; pulse-radiolysis of Ar-purged aqueous solution containing only acetone; sensitivity map; spectra and concentrations versus time of $Br_2^{\bullet-}$ and $BrOH^{\bullet-}$ obtained with the optimal set of parameters MAP2; full references 40 and 41. This information is available free of charge via internet at http://pubs.acs.org.

AUTHOR INFORMATION

Corresponding Author

* Tel.: +33 (0)169154511, Fax: +33 (0)169156188, E-mail: isabelle.lampre@u-psud.fr (I.L.)

Notes

The authors declare no competing financial interest.

ACKNOWLEDGMENT

The authors thank Dr B. Levy for fruitful discussions.

REFERENCES

(1) Rafi, A.; Sutton, H. C., Radiolysis of aerated solutions of potasium bromide. *Trans. Faraday Soc.* **1965,** 61, 877-890.

(2) Sutton, H. C.; Adams, G. E.; Boag, J. W.; Michael, B. D., Radical yields and kinetics in pulse radiolysis of potassium bromide. In *Pulse radiolysis*, Ebert, M.; Keene, J. P.; Swallow, A.; Baxendale, J. H., Eds. Academic press: London, 1965; pp 61-81.

(3) Matheson, M. S.; Mulac, W. A.; Weeks, J. L.; Rabani, J., The pulse radiolysis of deaerated aqueous bromide solutions. *J. Phys. Chem.* **1966,** 70, (7), 2092-2099.

(4) Zehavi, D.; Rabani, J., Pulse radiolytic investigation of O_{aq}^- radical ions. *J. Phys. Chem.* **1971,** 75, (11), 1738-1744.

(5) Zehavi, D.; Rabani, J., The oxidation of aqueous bromide ions by hydroxyl radicals. A pulse radiolytic investigation. *J. Phys. Chem.* **1972,** 76, (3), 312-319.

(6) Behar, D., Pulse radiolysis studies on Br^- in aqueous solution: the mechanism of Br_2^- formation. *J. Phys. Chem.* **1972,** 76, (13), 1815-1818.

(7) Treinin, A.; Hayon, E., Charge transfer spectra of halogen atoms in water. Correlation of the electronic transition energies of iodine, bromine, chlorine, hydroxyl, and hydrogen radicals with their electron affinities. *J. Am. Chem. Soc.* **1975,** 97, (7), 1716-1721.

(8) Mamou, A.; Rabani, J.; Behar, D., On the oxidation of aqueous Br^- by OH radicals, studied by pulse radiolysis. *J. Phys. Chem.* **1977,** 81, (15), 1447-1448.

(9) D'Angelantonio, M.; Venturi, M.; Mulazzani, Q. G., A re-examination of the decay kinetics of pulse radiolytically generated Br_2^- radicals in aqueous solution. *Radiat. Phys. Chem.* **1988,** 32, (3), 319-324.

(10) Hug, G. L.; Wang, Y.; Schöneich, C.; Jiang, P.-Y.; Fessenden, R. W., Multiple time scales in pulse radiolysis. Application to bromide solutions and dipeptides. *Radiat. Phys. Chem.* **1999,** 54, 559-566.

(11) Baldacchino, G.; Vigneron, G.; Renault, J. P.; Le Caër, S.; Mialocq, J.-C.; Balanzat, E.; Bouffard, S., Hydroxyl radical yields in the tracks of high energy $^{13}C^{6+}$ and $^{36}Ar^{18+}$ ions in liquid water. *Nucl. Instr. and Meth. in Phys. Res. B* **2006,** 245, 288-291.

(12) Mirdamadi-Esfahani, M.; Lampre, I.; Marignier, J.-L.; De Waele, V.; Mostafavi, M., Radiolytic formation of tribromine ion Br_3^- in aqueous solutions, a system for steady-state dosimetry. *Radiat. Phys. Chem.* **2009,** 78, 106-111.

(13) Balcerzyk, A.; La Verne, J.; Mostafavi, M., Direct and indirect radiolytic effects in highly concentrated aqueous solutions of bromide. *J. Phys. Chem. A* **2011,** 115, 4326-4333.

(14) Lin, M.; Archirel, P.; Van-Oanh, N. T.; Muroya, Y.; Fu, H.; Yan, Y.; Nagaishi, R.; Kumagai, Y.; Katsumura, Y.; Mostafavi, M., Temperature dependence absorption spectra of Br^-, $Br_2^{\bullet-}$, and Br_3^- in aqueous solutions. *J. Phys. Chem. A* **2011,** 115, 4241-4247.

(15) Hug, G. L., *Optical spectra of nonmetallic inorganic transient species in aqueous solution*. Nat. Bur. Stand. (U.S.): Washington, 1981; Vol. NSRDS-NBS 69, p 52-53.

(16) Wang, T. X.; Kelley, M. D.; Cooper, J. N.; Beckwith, R. C.; Margerum, D. W., Equilibrium, kinetic, and UV-spectral characteristics of aqueous bromine chloride, bromine, and chlorine species. *Inorg. Chem.* **1994,** 33, (25), 5872-5878.

(17) Kläning, U. K.; Wolff, T., Laser flash photolysis of hypochlorous acid (HClO), hypochlorite (ClO^-), hypobromous acid (HBrO), and hypobromite(BrO^-) in aqueous solution. Reactions of chlorine and bromine atoms. *Ber. Bunsenges. Phys. Chem.* **1985,** 89, (3), 243-245.

(18) Lind, J.; Shen, X.; Eriksen, T. E.; Merényi, G.; Eberson, L., One-electron reduction of N-bromosuccinimide. Rapid expulsion of a bromine atom. *J. Am. Chem. Soc.* **1991,** 113, (12), 4629-4633.

(19) Merényi, G.; Lind, J., Reaction mechanism of hydrogen abstraction by the bromine atom in water. *J. Am. Chem. Soc.* **1994,** 116, (17), 7872-7876.

(20) Marov, I.; Symons, C. R., Unstable intermediates. Part LXXXII. Electron spin resonance spectra of the species Br_2^-, I_2^-, $BrOH^-$, and IOH^- in γ-irradiated frozen aqueous solutions of alkali-metal halides. *J. Chem. Soc. A* **1971**, 201-204.

(21) Buxton, G. V.; Greenstock, C. L.; Helman, W. P.; Ross, A. B., Critical review of rate constant of hydrated electrons, hydrogen atoms and hydroxyl radicals in aqueous solution. *J. Phys. Chem. Ref. Data* **1988,** 17, 513-886.

(22) Le Caer, S.; Heninger, M.; Pernot, P.; Mestdagh, H., Successive reactions of iron carbonyl cations with dimethyl ether: direct cleavage versus rearrangement. *Phys. Chem. Chem. Phys.* **2002,** 4, 1855-1865.

(23) Renou, F.; Mostafavi, M.; Archirel, P.; Bonazzola, L.; Pernot, P., Solvated electron pairing with earth alkaline metals in THF. 1. Formation and structure of the pair with divalent magnesium. *J. Phys. Chem. A* **2003,** 107, 1506-1516.

(24) Renou, F.; Pernot, P.; Bonin, J.; Lampre, I.; Mostafavi, M., Solvated electron pairing with earth alkaline metals in THF. 2. Reactivity of the (Mg^{II}, e_s^-) pair with aromatic and halogenated hydrocarbon compounds. *J. Phys. Chem. A* **2003,** 107, 6587-6593.

(25) Mozziconacci, O.; Mirkowski, J.; Rusconi, F.; Pernot, P.; Bobrowski, K.; Houée-Levin, C., Superoxide radical anions protect enkephalin from oxidation if the amine group is blocked. *Free Rad. Biol. Med.* **2007,** 43, 229-240.

(26) Soroushian, B.; Lampre, I.; Bonin, J.; Pernot, P.; Pommeret, S.; Mostafavi, M., Solvation dynamics of the electron produced by two-photon ionization of liquid polyols. I. Ethylene glycol. *J. Phys. Chem. A* **2006,** 110, 1705-1717.

(27) Bonin, J.; Lampre, I.; Pernot, P.; Mostafavi, M., Solvation dynamics of electron produced by two-photon ionization of liquid polyols. II. Propanediols. *J. Phys. Chem. A* **2007,** 211, 4902-4913.

(28) Bonin, J.; Lampre, I.; Pernot, P.; Mostafavi, M., Solvation dynamics of electron produced by two-photon ionization of liquid polyols. III. Glycerol. *J. Phys. Chem. A* **2008,** 112, 1880-1886.

(29) Schmidhammer, U.; Pernot, P.; De Waele, V.; Jeunesse, P.; Demarque, A.; Murata, S.; Mostafavi, M., Distance dependence of the reaction rate for the reduction of metal cations by solvated electrons: a picosecond pulse radiolysis study. *J. Phys. Chem. A* **2010,** 114, 12042-12051.

(30) El Omar, K.; Schmidhammer, U.; Jeunesse, P.; Larbre, J.-P.; Lin, M.; Muroya, Y.; Katsumura, Y.; Pernot, P.; Mostafavi, M., Time-Dependent Radiolytic Yield of OH• Radical Studied by Picosecond Pulse Radiolysis. *J. Phys. Chem. A* **2011,** 115, 12212-12216.

(31) Marignier, J.-L.; De Waele, V.; Monard, H.; Gobert, F.; Larbre, J.-P.; Demarque, A.; Mostafavi, M.; Belloni, J., Time-resolved spectroscopy at picisecond laser-triggered electron accelerator ELYSE. *Radiat. Phys. Chem.* **2006,** 75, 1024-1033.

(32) Belloni, J.; Crowell, R. A.; Katsumura, Y.; Lin, M.; Marignier, J. L.; Mostafavi, M.; Muroya, Y.; Saeki, A.; Tagawa, S.; Yoshida, Y.; De Waele, V.; Wishart, J. F., Ultrafast pulse radiolysis methods. In *Radiation trends in radiation chemistry*, Wishart, J. F.; Rao, B. S. M., Eds. World Scientific Publishing, Co. Lte. Ptd.: Singapore, 2010; pp 121-160.

(33) Herren, R.; Bazouin, J. R.; Marignier, J. L. Light flash generatoir, absorption spectrometer including such a generator and method for generating light flashes. 097068993, 2012.

(34) Gregory, P. C., *Bayesian logical data analysis for the physical sciences: a comparative approach with Mathematica support*. Cambridge University Press: Cambridge, 2005.

(35) Ruckebusch, C.; Sliwa, M.; Pernot, P.; de Juan, A.; Tauler, R., Comprehensive data analysis of femtosecond transient absorption spectra: a review. *J. Photochem. Photobiol. C: Photochem. Rev.* **2012,** 13, 1-27.

(36) Gelman, A.; Carlin, J. B.; Stern, H. C.; Rubin, D. B., *Bayesian data analysis*. Second ed.; Chapman & Hall / CRC: 2004.

(37) BIPM; IEC; IFCC; ILAC; ISO; IUPAC; IUPAP; OIML, *Evaluation of measurement data - Supplement 1 to the "Guide to the expression of uncertainty in measurement" - Propagation of distributions using a Monte Carlo method*. Joint Committee for Guides in Metrology, JCGM: 2008; Vol. 101.

(38) R Development Core Team *R: A language and environment for statistical computing*, R Foundation for Statistical Computing: Vienna, Austria, 2012, ISBN 3-900051-07-0, URL http://www.R-project.org/.

(39) Fuentealba, P.; Preuss, H.; Stoll, H.; von Szentpály, L., A proper account of core-polarization with pseudopotentials: single valence-electron alkali compounds. *Chem. Phys. Lett.* **1982,** 89, 418-422.

(40) Frisch, M. J.; Trucks, G. W.; Schlegel, H. B.; Scuseria, G. E.; Robb, M. A.; Cheeseman, J. R.; Scalmani, G.; Barone, V.; Mennucci, B.; Petersson, G. A. et al., *Gaussian 09, revision A.02*, Gaussian, Inc.: Wallingford CT, 2009.

(41) Werner, J.-J.; Kwoles, P. J.; Knizia, G.; Manby, F. R.; Schütz, M.; Celani, P.; Korona, T.; Lindh, R.; Mitrushenkov, A.; Rauhut, G. et al., *MOLPRO* University College Cardiff Consultants Limited: 2010.

(42) Kasama, K.; Takematsu, A.; Arai, S., Photochemical reactions of triplet acetone with indole, purine and pyrimidine derivatives. *J. Phys. Chem.* **1982,** 86, 2420-2427.

(43) Mills, G.; Henglein, A., Radiation chemistry of Na_3IrCl_6 solutions: catalysed H_2 formation by radicals and postirradiation reduction of $IrCl_6^{3-}$ by propanol-2. *Radiat. Phys. Chem.* **1985,** 26, 391-399.

(44) Laroff, G. P.; Fessenden, R. W., Equilibrium and kinetics of the acid dissociation of several hydroxyalkyl radicals. *J. Phys. Chem.* **1973,** 77, 1283-1288.

(45) Wolfenden, B. S.; Wilson, R. L., Radical-cations as reference chromogens in kinetic studies of one-electron transfer reactions: pulse radiolysis studies of 2,2′-azinobis-(3-ethylbenzthiazoline-6-sulphonate). *J. Chem. Soc., Perkin Trans. 2* **1982**, 805-812.

(46) Barat, F.; Gilles, L.; Hickel, B.; Lesigne, B., Effect of the dielectric constant on the reactivity of the solvated electron. *J. Phys. Chem.* **1973,** 77, 1711-1715.

(47) Afanassiev, A. M.; Okazaki, K.; Freeman, G. R., Effect of solvation energy on electron reaction rates in hydroxylic solvents. *J. Phys. Chem.* **1979,** 83, 1244-1249.

(48) Philips, G. O.; Wedlock, D. J.; Micic, O. I.; Milosavljevic, B. H.; Thomas, J. K., Radiation induced diffusion controlled reactions. A probe for enhanced solute diffusion in polysaccharide matrices. *Radiat. Phys. Chem.* **1980,** 15, 187-193.

(49) Idriss-Ali, K. M.; Freeman, G. R., Electron behavior in mixed solvents: optical spectra and reactivities in water/alkane diols. *Can. J. Chem.* **1984,** 62, 2217-2222.

(50) Maham, Y.; Freeman, G. R., Effect of solvent structure on the electron reactivity: 1-propanol/water mixtures. *J. Phys. Chem.* **1985**, (89), 4347-4352.

(51) Lai, C. C.; Freeman, G. R., Solvent effects on the reactivity of solvated electrons with organic solutes in methanol/water and ethanol/water mixed solvents. *J. Phys. Chem.* **1990,** 94, 302-308.

(52) Saltelli, A.; Chan, K.; Scott, E. M., *Sensitivity Analysis*. Wiley: 2000.

(53) Zhang, H.-X.; Goutsias, J., A comparison of approximation techniques for variance-based sensitivity analysis of biochemical reaction systems. *BMC Bioinformatics* **2010,** 11, 246.

(54) Martins, M. A. F.; Requião, R.; Kalid, R. A., Generalized expressions of second and third order for the evaluation of standard measurement uncertainty. *Measurement* **2011,** 44, 1526-1530.

(55) Archirel, P., Unpublished results.

(56) Pathak, A. K.; Mukherjee, T.; Maity, D. K., Theoretical studies on photoelectron and IR spectral properties of $Br2^{\cdot-}(H_2O)_n$ clusters. *J. Chem. Phys.* **2007,** 127, 044304.

(57) Becke, A. D., Density-functional thermochemistry. III. The role of exact exchange. *J. Chem. Phys.* **1993,** 98, 5648-5652.

Table 1. **Values of the optimized parameters at the various stages of the process**.

Parameter	***Prior* pdf**	**MAP(1)**	**MAP(2)**	**MCMC Mean**	**MCUP**
δt (ns)	Norm(28, 2)	21	27	27.3 (12)	27.17 (70)
$[OH^{\bullet}]_0$ ($\times 10^{-5}$ M)	Lnorm(2, 50%)	2.3	2.15	2.21 (4%)	2.221 (4%)
$[Br^-]_0$ (M)	Lnorm(0.010, 5%)	0.098	0.010	0.010 (4%)	0.010 (2%)
$\varepsilon_{max}(Br_2^{\bullet -})$ ($dm^3\ mol^{-1}\ cm^{-1}$)	Norm(9900, 300)	9548	9707	9700 (260)	9700 (25)
k_1 ($\times 10^{10}\ M^{-1}\ s^{-1}$)	Lnorm(1.1, 10%)	fixed	0.85	0.84 (6%)	0.84 (5%)
k_{-1} ($\times 10^{7}\ s^{-1}$)	Lnorm(3.3, 20%)	fixed	2.77	2.77 (10%)	2.77 (6%)
k_2 ($\times 10^{6}\ s^{-1}$)	Lnorm(4.2, 20%)	fixed	8.33	8.17 (8%)	8.01 (7%)
k_{10} ($\times 10^{8}\ M^{-1}\ s^{-1}$)	Lnorm(1.3, 20%)	fixed	1.64	1.69 (8%)	1.70 (6%)
χ^2_R		1.06	1.02	-	1.022 (1)
P		0.01	0.13	-	-

Norm(x,σ) corresponds to a normal or Gaussian distribution with x the location of the peak and σ the standard deviation; Lnorm(x,y%) stands for *Lognormal* distributions with x the mean and uncertainty factor taken as a percentage y%; χ^2_R is the reduced chi-square, i.e. the sum of the weighted residuals divided by the number of degrees of freedom (NDF); P is the probability for a χ^2_R issued from a chi-square distribution with the same NDF to be larger than the reported value.

Table 2. Spectral properties of $Br_2^{\bullet-}$ and $BrOH^{\bullet-}$ derived by Gaussian fit in the energy scale of the numerical spectra generated by the MCMC and MCUP procedures.

Derived Spectral Properties	MCMC	MCUP
$\varepsilon_{max}(Br_2^{\bullet-})$ ($dm^3\ mol^{-1}\ cm^{-1}$)	9600(260)	9540(30)
$\lambda_{max}(Br_2^{\bullet-})$ (nm)	354.0	354.0
$\Delta\lambda(Br_2^{\bullet-})$ (nm)	38.122(50)	38.139(40)
$OS(Br_2^{\bullet-})$	7.32(20)	7.278(16)
$\varepsilon_{max}(BrOH^{\bullet-})$ ($dm^3\ mol^{-1}\ cm^{-1}$)	7800(365)	7800(140)
$\lambda_{max}(BrOH^{\bullet-})$ (nm)	352.32(10)	352.363(40)
$\Delta\lambda(BrOH^{\bullet-})$ (nm)	43.71(12)	43.279(80)
$OS(BrOH^{\bullet-})$	6.87(33)	7.02(17)
$OS(BrOH^{\bullet-}) / OS(Br_2^{\bullet-})$	0.938(32)	0.964(25)

ε_{max} and λ_{max} correspond to the maximum value of the extinction coefficient and its the position, respectiveley; $\Delta\lambda$ represents half the full width at half maximum (fwhm/2) of the absorption band ; OS stands for the oscillator strength.

Table 3. TDDFT results for $Br_2^{\bullet-}$ with two functionals and two basis sets.

functional	basis	ΔE (eV)	λ (nm)	OS
BHHLYP	pSDD	3.17	391	0.4976
BHHLYP	pSDD + diff	3.14	394	0.4868
B3LYP	pSDD	3.33	372	0.4554
B3LYP	pSDD + diff	3.31	374	0.4432

ΔE and λ represent the transition energy and wavelength, respectively; OS is the associated oscillator strength.

Table 4. TDDFT results for low lying conformations of $Br_2^{\bullet-}(H_2O)_n$ obtained with B3LYP and the pSDD basis set.

n	ΔE (eV)	λ (nm)	OS
0	3.33	372	0.45
1	3.33	372	0.42
2	3.44	360	0.43
3	3.42	363	0.43
4	3.41	364	0.42
Exp.	-	355	-

ΔE and λ represent the transition energy and wavelength, respectively; OS is the associated oscillator strength.

Table 5. TDDFT results for low lying conformations of $BrOH^{\bullet-}(H_2O)_n$. The results are obtained with B3LYP and the pSDD basis set.

n	ΔG (eV)	binding mode (n_{conf})	ΔE (eV)	λ (nm)	OS
0	-	-	3.07	404	0.34
1	0.	W → OH (2)	3.37	368	0.35
1	+0.025	W → Br (3)	3.19	388	0.34
1	+0.084	W ← OH (1)	3.11	398	0.35
2	-	-	3.51	354	0.34
3	-	-	3.50	354	0.33
4	-	-	3.52	353	0.32
Exp.	-	-	-	355	-

ΔG is the energy difference between the $BrOH^{\bullet-}(H_2O)$ configurations where W stands for the water molecule; ΔE and λ represent the transition energy and wavelength, respectively; OS is the associated oscillator strength.

FIGURE CAPTION

Figure 1. (a) Optical absorption spectra recorded by pulse radiolysis of N_2-purged aqueous solutions containing 0.01 M NaBr and 0.1 M acetone at different time after the electron pulse; **(b)** Comparison between the normalized absorption spectra recorded at 10 ns and 400 ns.

Figure 2. Absorption signals obtained at different wavelengths by pulse radiolysis of N_2-purged aqueous solutions containing 0.01 M NaBr and 0.1 M acetone on two different time scales: **(a)** 50 ns, **(b)** 500 ns.

Figure 3. Optical absorption spectra recorded by pulse radiolysis of N_2-purged aqueous solutions containing 0.05 M NaBr and 0.1 M acetone at different time after the electron pulse.

Figure 4. Absorption signals obtained at different wavelengths recorded by pulse radiolysis of N_2-purged aqueous solutions containing 0.05 M NaBr and 0.1 M acetone on two different time scales: **(a)** 20 ns, **(b)** 500 ns.

Figure 5. Top left: Downsized spectrokinetic data matrix (the absorbance increases from dark blue to dark red); Top right: optimized absorbance matrix giving the best fit (see text for details); Bottom left: Residuals matrix; Bottom right: Q-Q plot comparing the residuals with their theoretical values.

Figure 6. Absorption spectra of $Br_2^{\bullet-}$ (black curve) and $BrOH^{\bullet-}$ (red curve) derived from the Bayesian data analysis of the experimental results in Figure 1. The best fit spectra are represented by bold lines.

Figure 7. Optimized most stable configurations of $Br_2^{\bullet-}(H_2O)_n$ with n = 1 to 4.

Figure 8. Optimized most stable configurations of $BrOH^{\bullet-}(H_2O)_n$ with n = 1 (three possibilities) and n = 2 to 4.

Figure 9. Calculated absorption spectra of $Br_2^{\bullet-}(H_2O)_3$ and $BrOH^{\bullet-}(H_2O)_3$ with empirical fwhm values.

Figure 1.

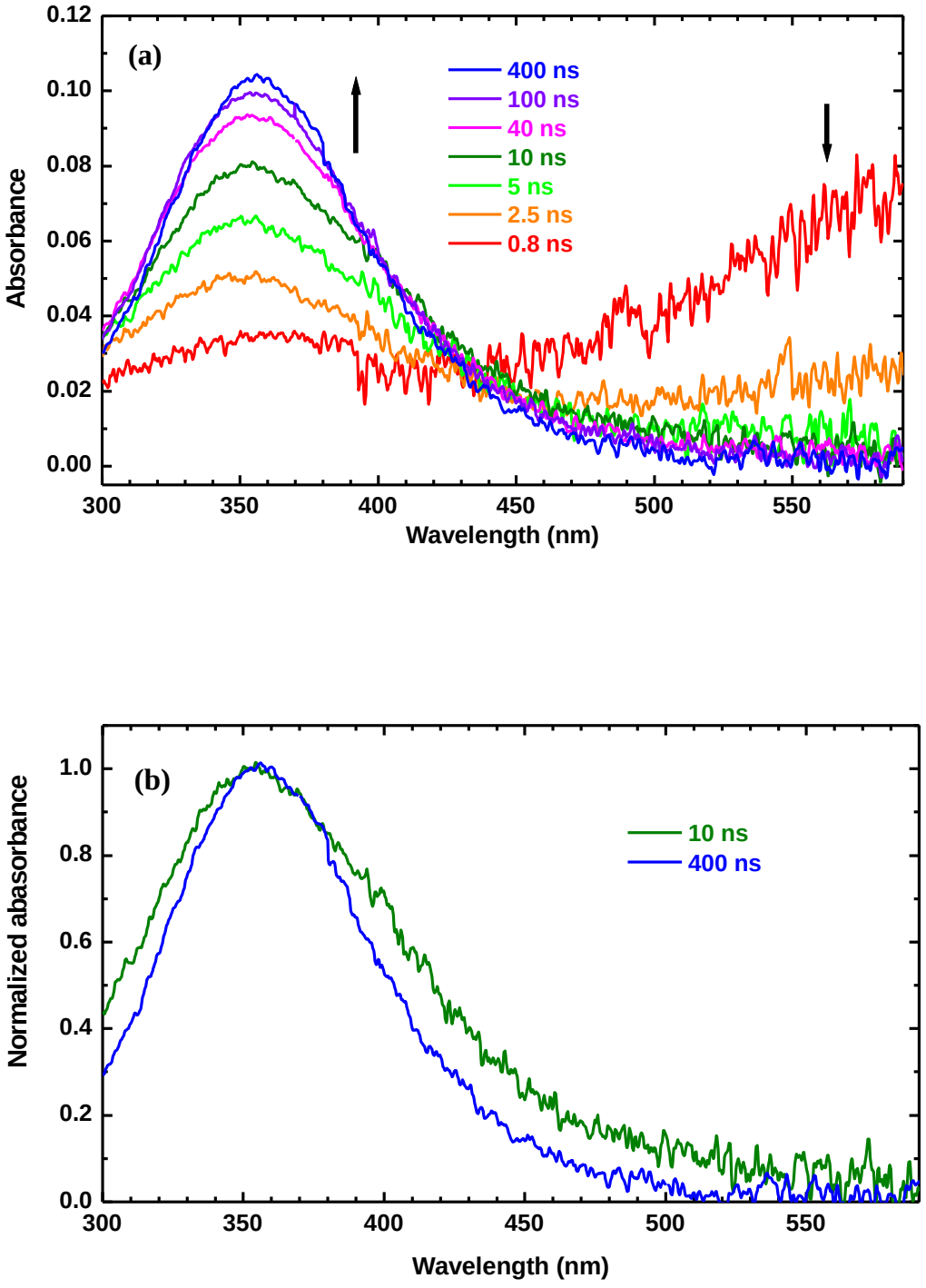
(a)
400 ns
100 ns
40 ns
10 ns
5 ns
2.5 ns
0.8 ns
Absorbance
Wavelength (nm)
0.12
0.10
0.08
0.06
0.04
0.02
0.00
300
350
400
450
500
550
(b)
10 ns
400 ns
Normalized abasorbance
Wavelength (nm)
1.0
0.8
0.6
0.4
0.2
0.0

Figure 2.

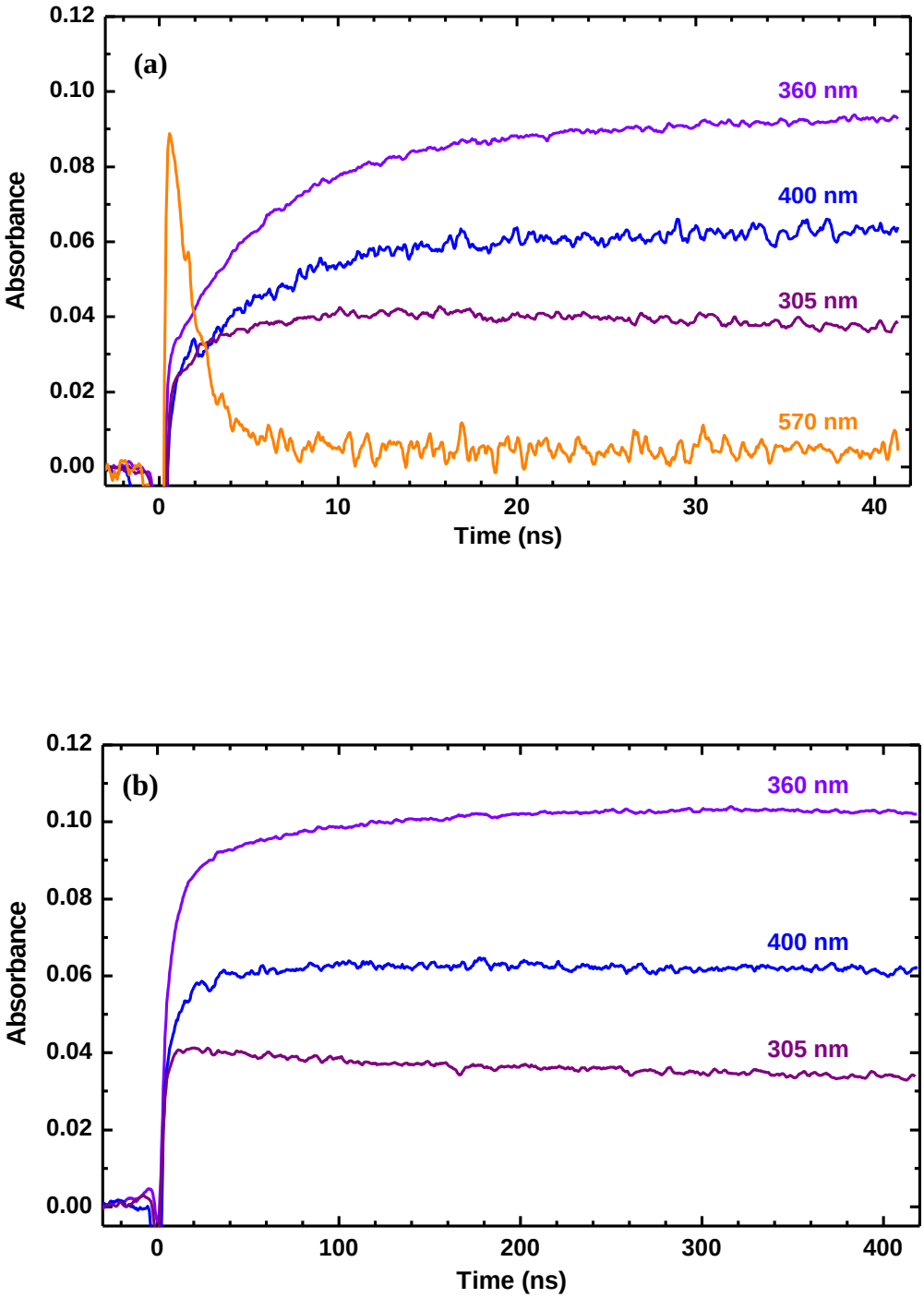
(a)
360 nm
400 nm
305 nm
570 nm
Absorbance
Time (ns)
0.12
0.10
0.08
0.06
0.04
0.02
0.00
0
10
20
30
40
(b)
360 nm
400 nm
305 nm
Absorbance
Time (ns)
0.12
0.10
0.08
0.06
0.04
0.02
0.00
0
100
200
300
400

Figure 3.

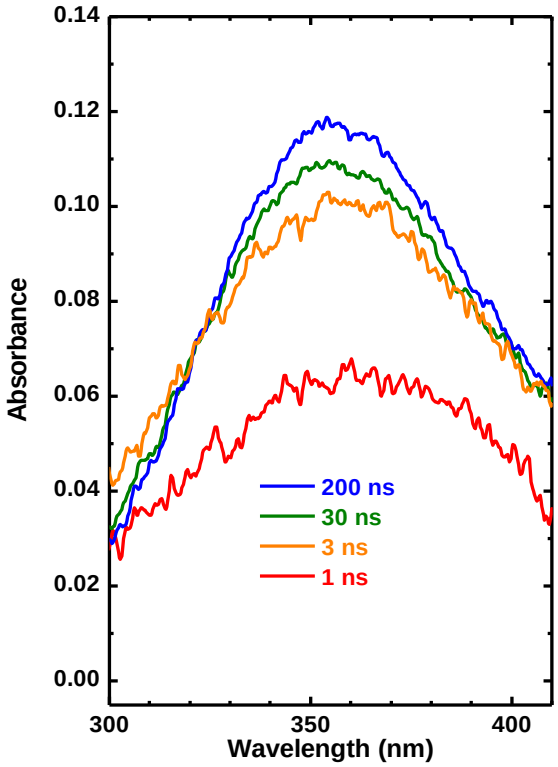
0.14
0.12
0.10
0.08
0.06
0.04
0.02
0.00
Absorbance
300
350
400
Wavelength (nm)
200 ns
30 ns
3 ns
1 ns

Figure 4.

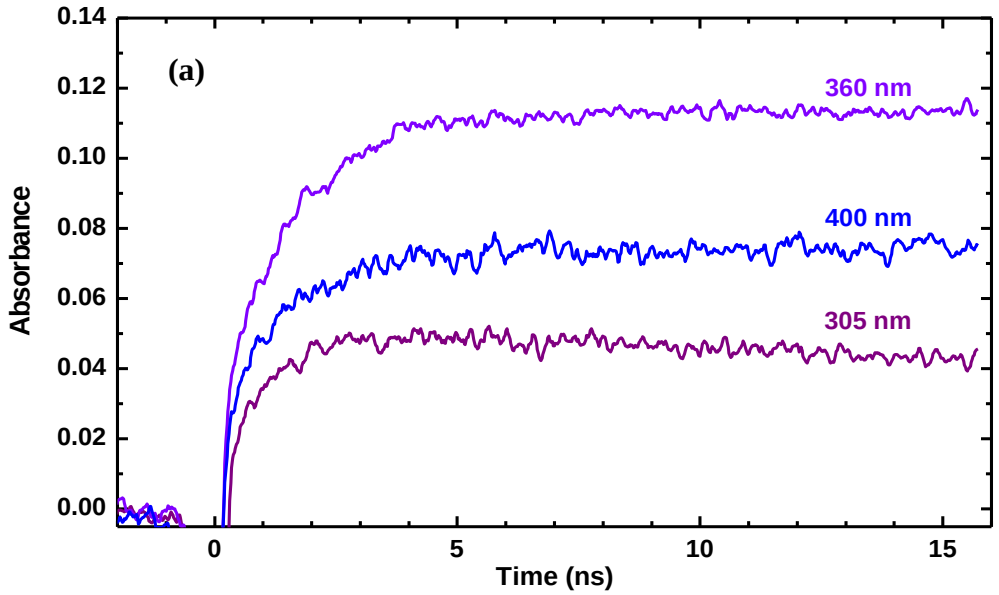
(a)
360 nm
400 nm
305 nm
Absorbance
Time (ns)
0.14
0.12
0.10
0.08
0.06
0.04
0.02
0.00
0
5
10
15

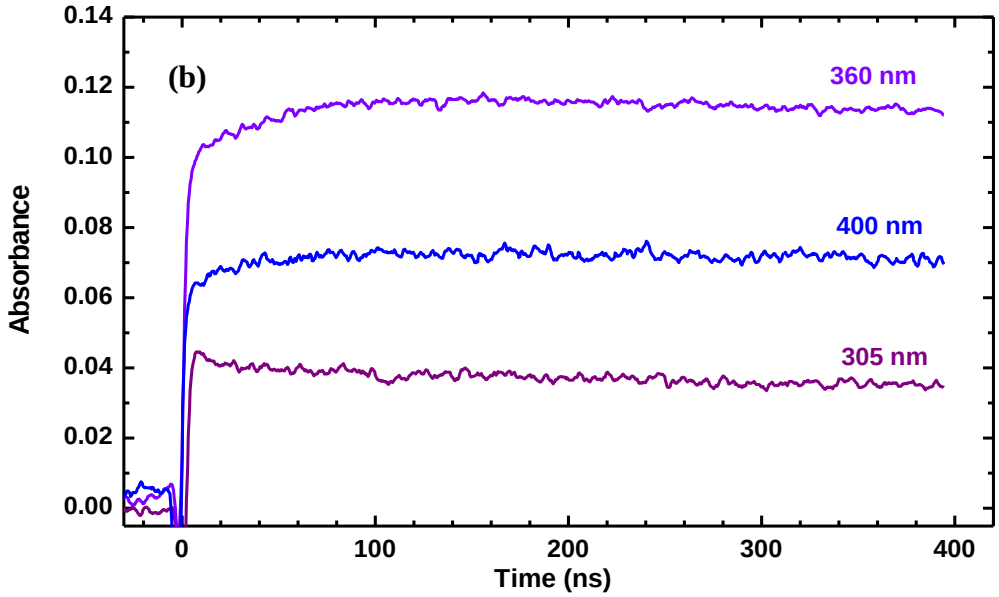
(b)
360 nm
400 nm
305 nm
Absorbance
Time (ns)
0.14
0.12
0.10
0.08
0.06
0.04
0.02
0.00
0
100
200
300
400

Figure 5.

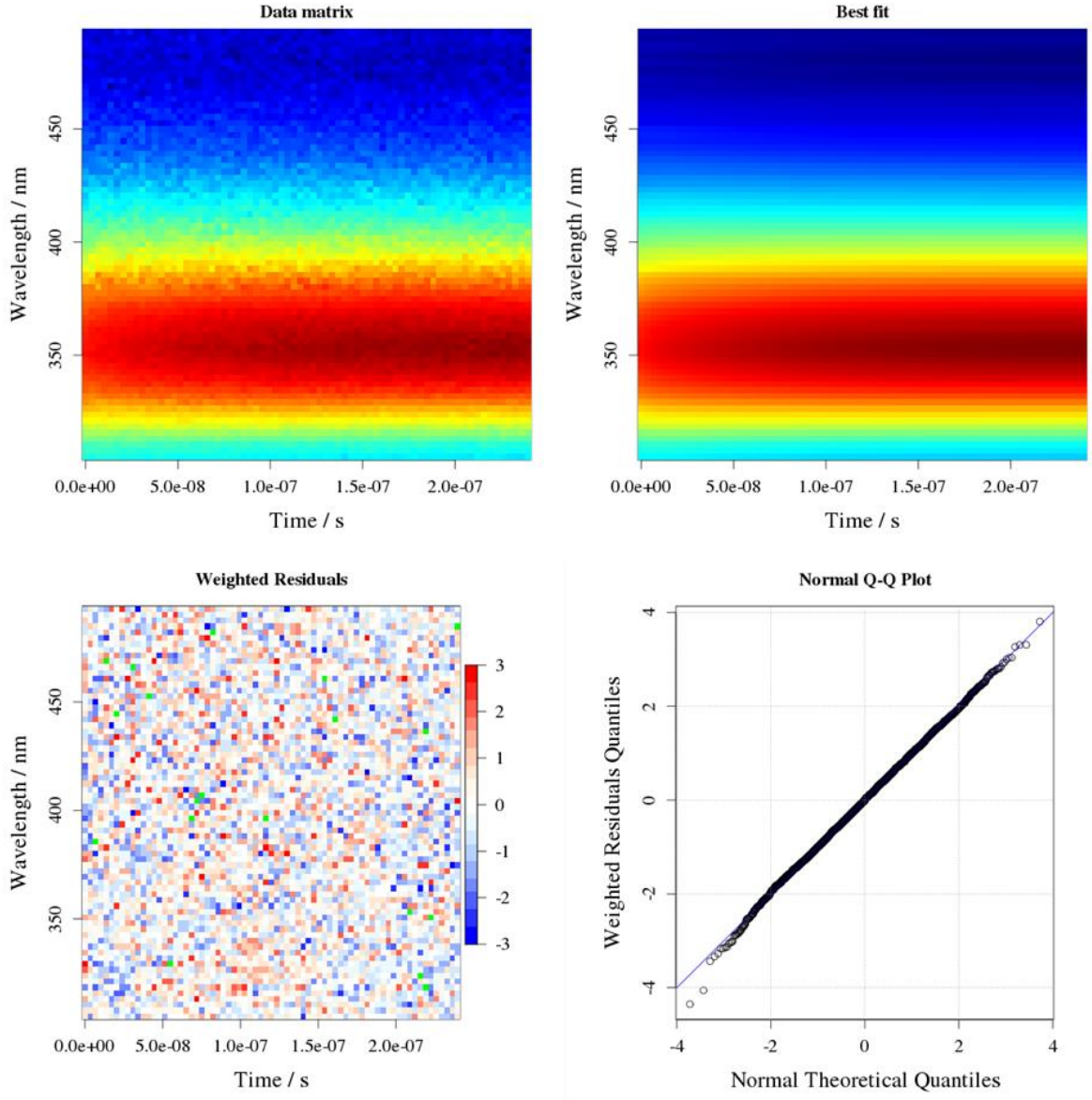
Data matrix
Best fit
Weighted Residuals
Normal Q-Q Plot
Wavelength / nm
Time / s
Weighted Residuals Quantiles
Normal Theoretical Quantiles
0.0e+00
5.0e-08
1.0e-07
1.5e-07
2.0e-07
350
400
450
-4
-2
0
2
4
-3
-2
-1
0
1
2
3

Figure 6.

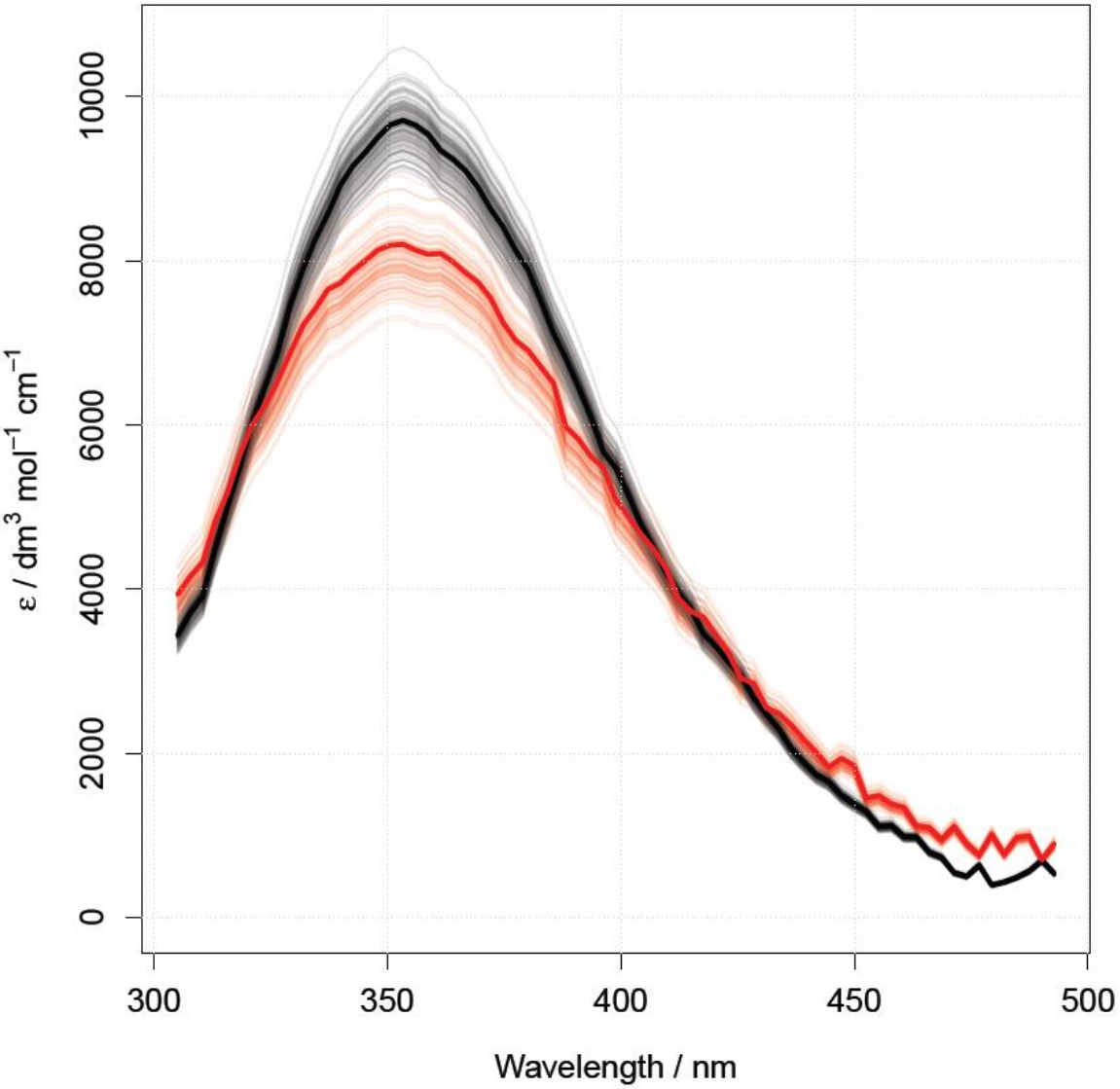
ε / dm3 mol−1 cm−1
0
2000
4000
6000
8000
10000
300
350
400
450
500
Wavelength / nm

Figure 7.

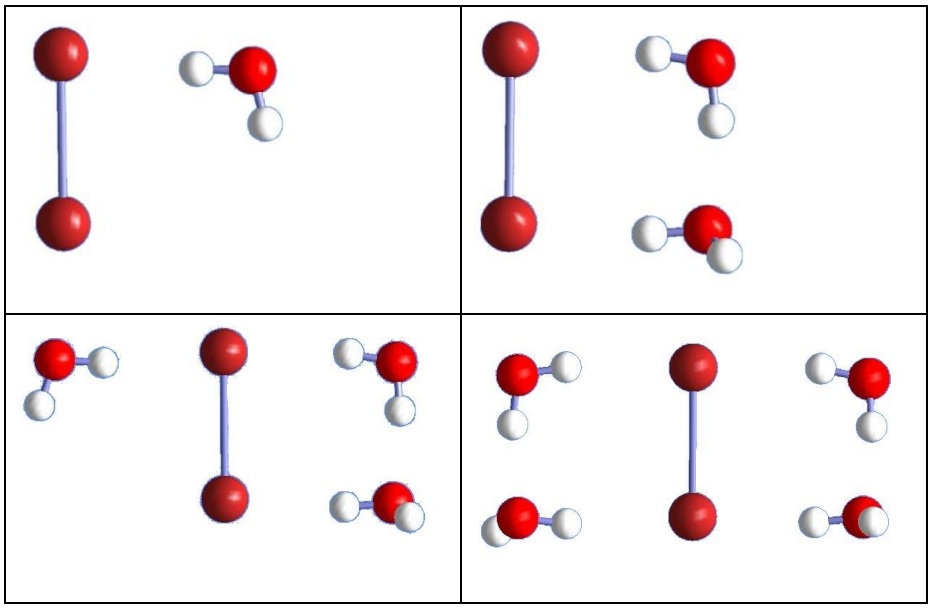

Figure 8.

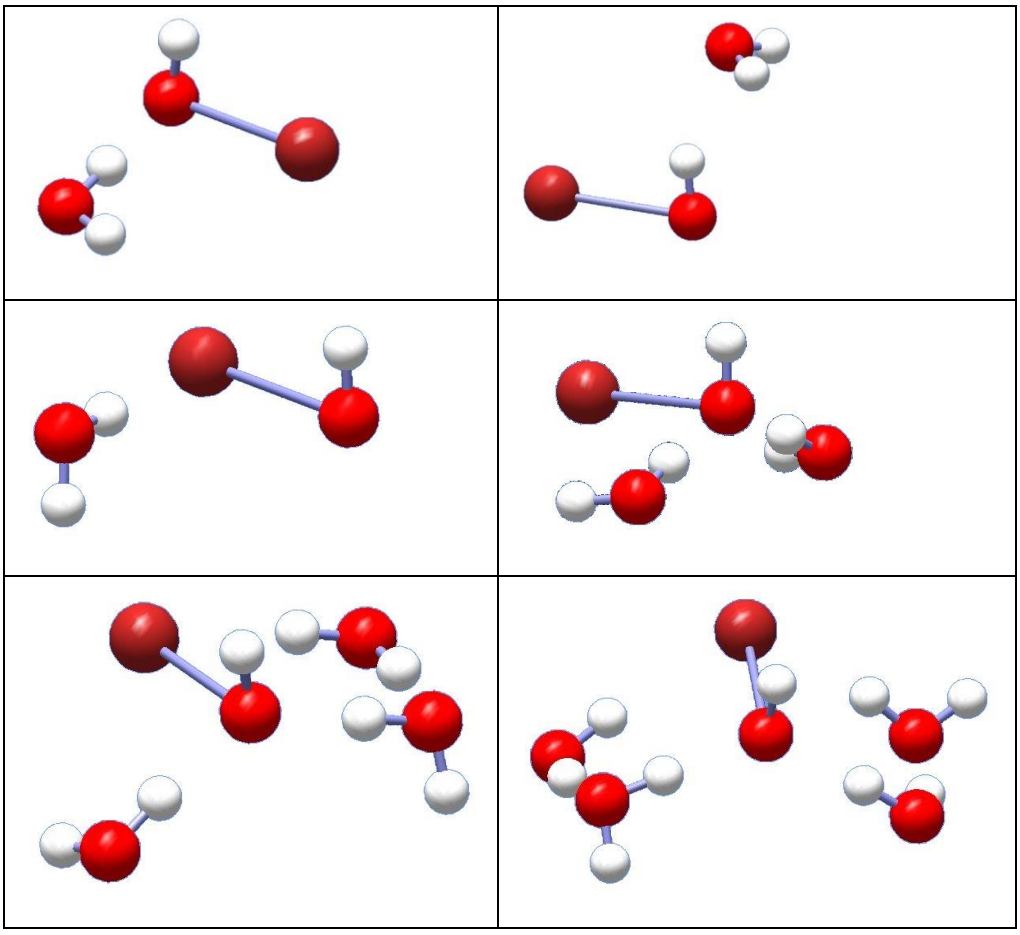

Figure 9

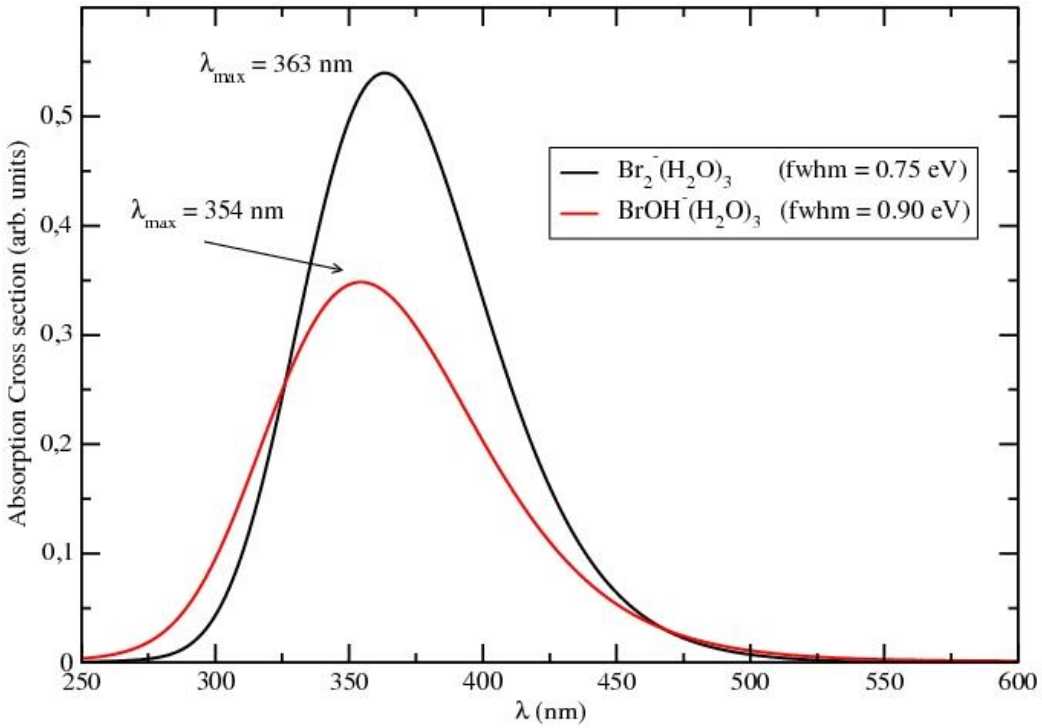
λmax = 363 nm
λmax = 354 nm
Br2-(H2O)3 (fwhm = 0.75 eV)
BrOH-(H2O)3 (fwhm = 0.90 eV)
Absorption Cross section (arb. units)
λ (nm)
0
0,1
0,2
0,3
0,4
0,5
250
300
350
400
450
500
550
600

TOC Graphic

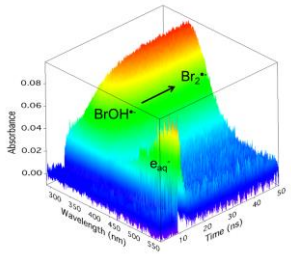
Br2•-
BrOH•-
eaq-
Absorbance
0.08
0.06
0.04
0.02
0.00
300
350
400
450
500
550
Wavelength (nm)
10
20
30
40
50
Time (ns)

Supporting Information

Oxidation of Bromide Ions by Hydroxyl Radicals: Spectral Characterization of the Intermediate $BrOH^{\bullet-}$

Isabelle Lampre[*]*, Jean-Louis Marignier, Malaknaz Mirdamadi-Esfahani, Pascal Pernot, Pierre Archirel and Mehran Mostafavi*

Laboratoire de Chimie Physique, UMR 8000 CNRS / Université Paris-Sud, Faculté des Sciences d'Orsay, Bât. 349, 91405 Orsay Cedex, France

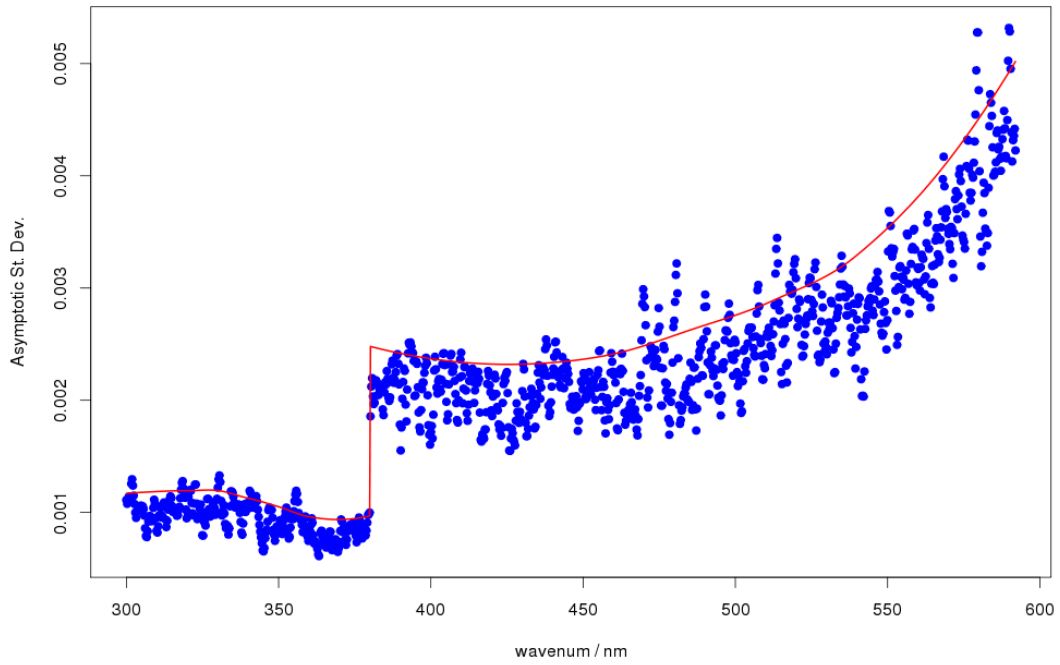

Figure S1: Wavelength-dependence of noise in data. The dots are the standard deviation calculated over 200 points at late time/delay. The red curve represents the 90% probability upper bound for the noise amplitude.

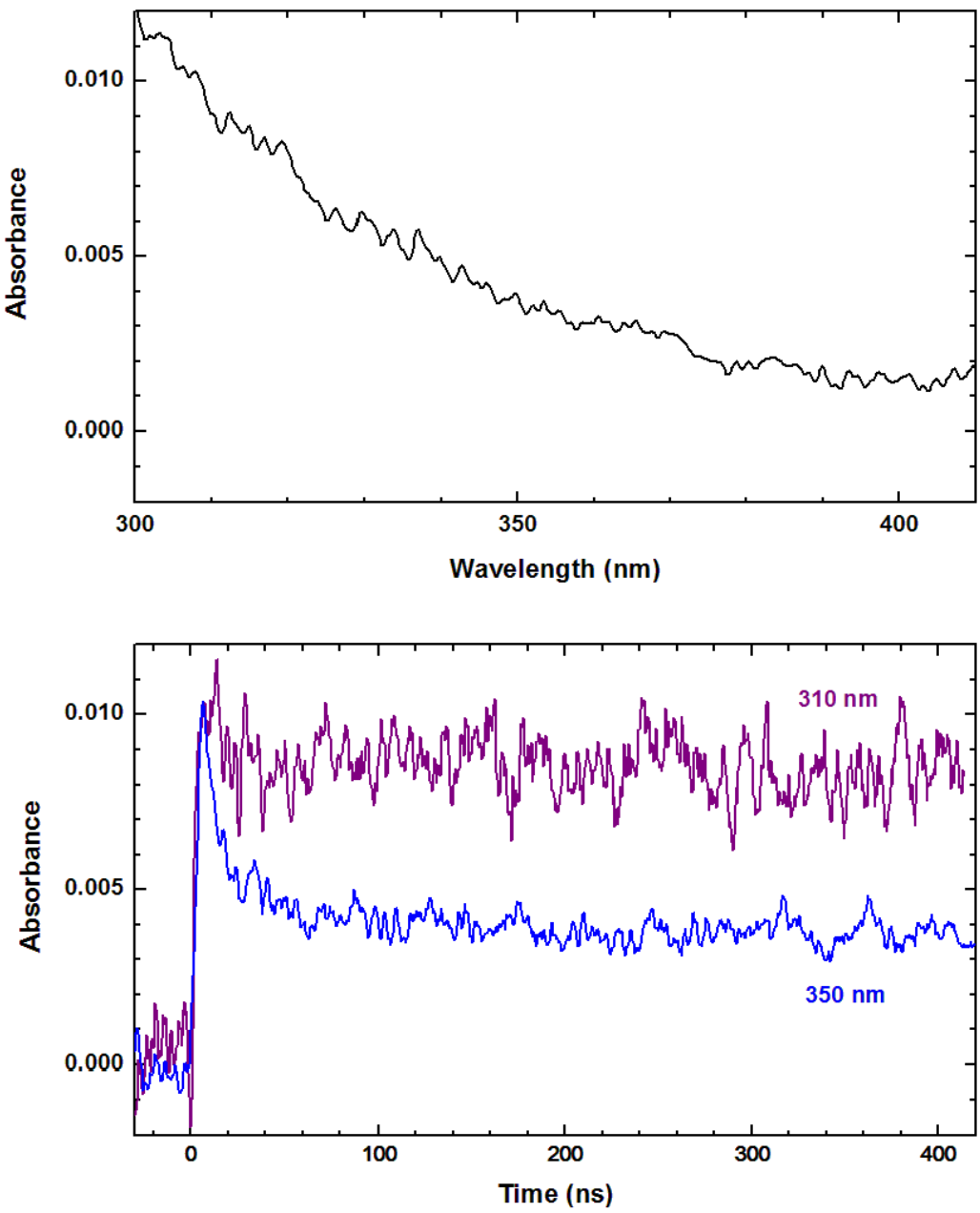

Figure S2: Optical absorption spectrum (top) and time-dependent signals (bottom) obtained by pulse radiolysis of N_2-purged aqueous solutions containing 0.1 M acetone.

The found spectrum corresponds to that of the protonated radical, $(CH_3)_2C^{\bullet}OH$, generated by the reaction between acetone and hydrated electron (R8-9), as reported in the literature (Kasama, K.; Takematsu, A.; Arai, S. *J. Phys. Chem.* **1982**, *86*, 2420-2427; Mills, G.; Henglein, A. *Radiat. Phys. Chem.* **1985**, *26*, 391-399). The fast rise in absorbance during the pulse duration is due to the solvated electron. Then, the disappearance of the solvated electron is observed at 350 nm where its extinction coefficient is greater than that of $(CH_3)_2C^{\bullet}OH$, but it is not detected at 310 nm where the extinction coefficients are similar.

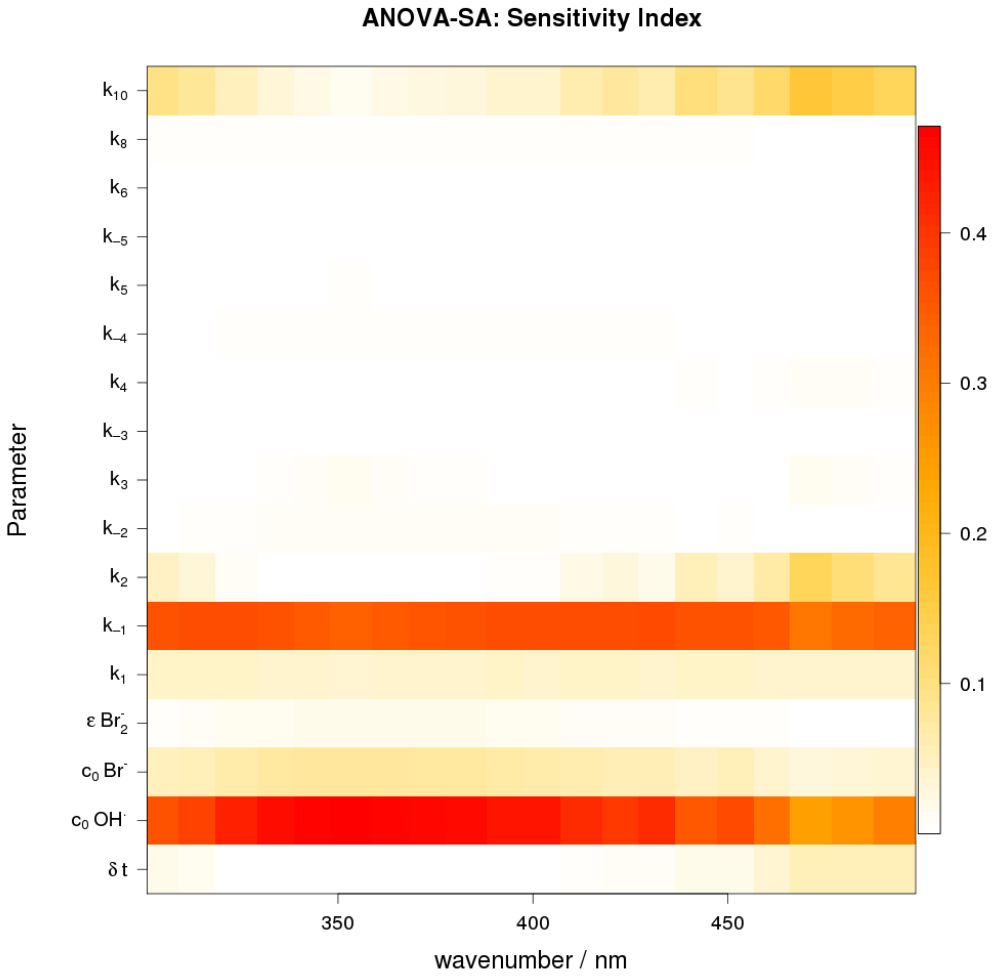

Figure S3: Sensitivity map.

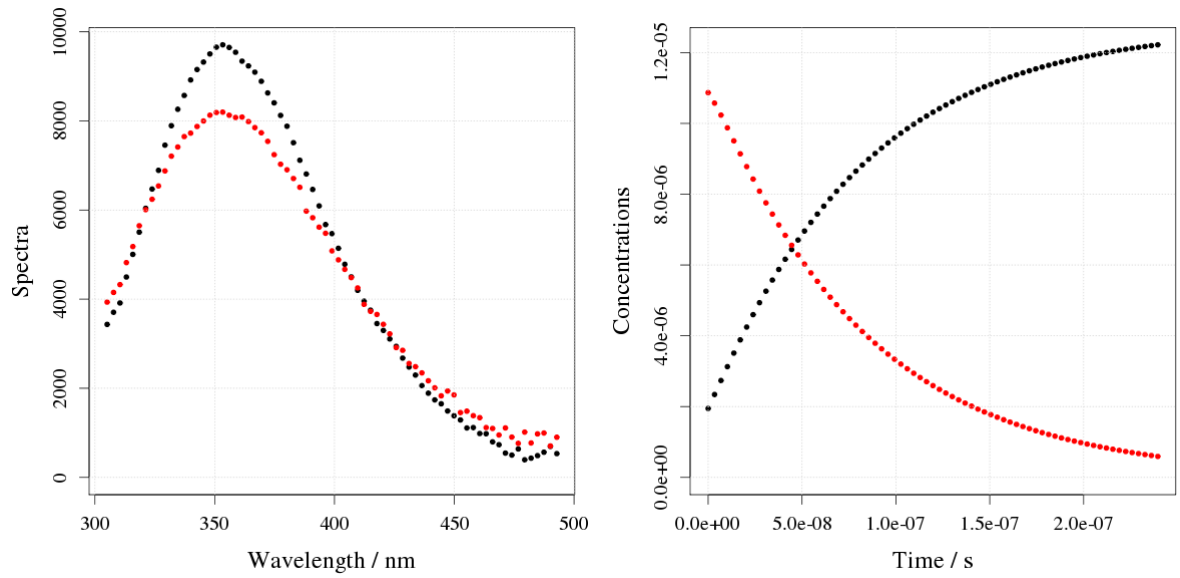

Figure S4: Absorption spectra (left) and concentrations versus time (right) of $Br_2^{\bullet-}$ (black dots) and $BrOH^{\bullet-}$ (red dots) obtained with the optimal set of parameters MAP2 during the Bayesian data analysis of the experimental results in Figure 1.

Full references

(40) Frisch, M. J.; Trucks, G. W.; Schlegel, H. B.; Scuseria, G. E.; Robb, M. A.; Cheeseman, J. R.; Scalmani, G.; Barone, V.; Mennucci, B.; Petersson, G. A.; Nakatsuji, H.; Carito, M.; Li, X.; Hratchian, H. P.; Izmaylov, A. F.; Bloino, J.; Zheng, G.; Sonnenberg, J. L.; Hada, M.; Ehara, M.; Toyota, K.; Fukuda, R.; Hasegawa, J.; Ishida, M.; Nakajima, T.; Honda, Y.; Kitao, O.; Nakai, H.; Vreven, T.; Montgomery, J. A. J.; Peralta, J. E.; Ogliaro, F.; Bearpark, M.; Heyd, J. J.; Brothers, E.; Kudin, K. N.; Staroverov, V. N.; Kobayashi, R.; Normand, J.; Raghavachari, K.; Rendell, A.; Burant, J. C.; Iyengar, S. S.; Tomasi, J.; Cossi, M.; Rega, N.; Millam, J. M.; Klene, M.; Knox, J. E.; Cross, J. B.; Bakken, V.; Adamo, C.; Jaramillo, J.; Gomperts, R.; Stratmann, R. E.; Yazyev, O.; Austin, A. J.; Cammi, R.; Pomelli, C.; Ochterski, J. W.; Martin, R. L.; Morokuma, K.; Zakrzewski, V. G.; Voth, G. A.; Salvador, P.; Dannenberg, J. J.; Dapprich, S.; Daniels, A. D.; Farkas, O.; Foresman, J. B.; Ortiz, J. V.; Cioslowski, J.; Fox, D. J. Gaussian 09, revision A.02; Gaussian, Inc.: Wallingford CT, 2009.

(41) Werner, J.-J.; Kwoles, P. J.; Knizia, G.; Manby, F. R.; Schütz, M.; Celani, P.; Korona, T.; Lindh, R.; Mitrushenkov, A.; Rauhut, G.; Shamasundar, K. R.; Adler, T. B.; Amos, R. D.; Bernhardsson, A.; Berning, A.; Cooper, D. L.; Deegan, M. J. O.; Dobbyn, A. J.; Eckert, F.; Goll, E.; Hampel, C.; Hesselmann, A.; Hetzer, G.; Hrenar, T.; Jansen, G.; Köppl, C.; Liu, Y.; Lloyd, A. W.; Mata, R. A.; May, A. J.; McNicholas, S. J.; Meyer, W.; Mura, M. E.; Nicklaβ, A.; O'Neill, D. P.; Palmieri, P.; Peng, D.; Pflüger, K.; Pitzer, R.; Reiher, M.; Shiozaki, T.; Stoll, H.; Stone, A. J.; Tarroni, R.; Thorsteinsson, T.; Wang, M. MOLPRO University College Cardiff Consultants Limited, 2010.